Article

Cell Reports

Myocardial Infarction Primes Autoreactive T Cells through Activation of Dendritic Cells

Graphical Abstract

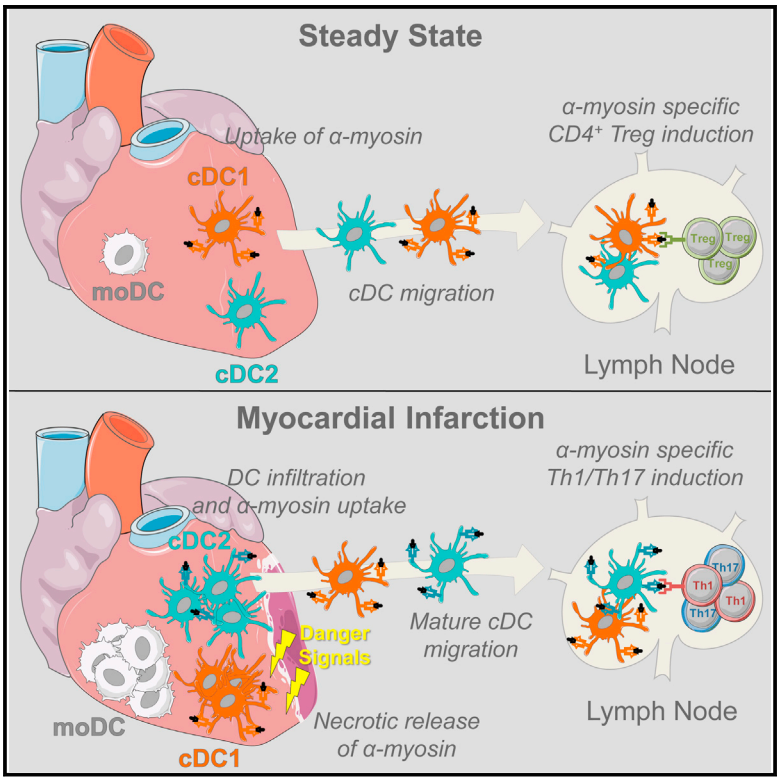

Highlights

- IRF8$^+$ cDC1, IRF4$^+$ cDC2, moDCs, and macrophages are the APCs of the murine heart
- Self-antigen presentation in the steady state drives Treg development via cDC1s
- Myocardial infarction promotes infiltration, activation, and maturation of all DCs
- Myocardial infarction promotes priming of Th1/Th17 autoreactive T cells via cDC2s

Authors

Katrien Van der Borght, Charlotte L. Scott, Veronika Nindl, ..., Martin Guilliams, Peter Carmeliet, Bart N. Lambrecht

Correspondence

peter.carmeliet@vib-kuleuven.be (P.C.), bart.lambrecht@ugent.be (B.N.L.)

In Brief

Van der Borght et al. demonstrate that myocardial infarction induces the priming of autoreactive CD4$^+$ T cells specific for cardiac self-antigen α-myosin in the heart-draining lymph node through the maturation and migration of conventional dendritic cells. Using ex vivo co-culture systems, cDC2s are shown to be superior in presenting α-myosin.

Accession Numbers

GSE94949

Van der Borght et al., 2017, Cell Reports *18*, 3005–3017
March 21, 2017
http://dx.doi.org/10.1016/j.celrep.2017.02.079

Cell Reports
Article

Myocardial Infarction Primes Autoreactive T Cells through Activation of Dendritic Cells

Katrien Van der Borght,[1,2] Charlotte L. Scott,[1,4] Veronika Nindl,[5] Ann Bouché,[3] Liesbet Martens,[1,2,4] Dorine Sichien,[1,4] Justine Van Moorleghem,[1,2] Manon Vanheerswynghels,[1,2] Sofie De Prijck,[1,4] Yvan Saeys,[1,2,4] Burkhard Ludewig,[5] Thierry Gillebert,[2] Martin Guilliams,[1,4] Peter Carmeliet,[3,*] and Bart N. Lambrecht[1,2,6,7,*]

[1]Immunoregulation and Mucosal Immunology, VIB Center for Inflammation Research, 9052 Ghent, Belgium
[2]Department of Internal Medicine, Ghent University, 9000 Ghent, Belgium
[3]VIB Vesalius Research Center, 3000 Leuven, Belgium
[4]Department of Biomedical Molecular Biology, Ghent University, 9000 Ghent, Belgium
[5]Institute of Immunobiology, Kantonsspital St. Gallen, 9007 St. Gallen, Switzerland
[6]Department of Pulmonary Medicine, ErasmusMC, 3015 Rotterdam, the Netherlands
[7]Lead Contact
*Correspondence: peter.carmeliet@vib-kuleuven.be (P.C.), bart.lambrecht@ugent.be (B.N.L.)
http://dx.doi.org/10.1016/j.celrep.2017.02.079

SUMMARY

Peripheral tolerance is crucial for avoiding activation of self-reactive T cells to tissue-restricted antigens. Sterile tissue injury can break peripheral tolerance, but it is unclear how autoreactive T cells get activated in response to self. An example of a sterile injury is myocardial infarction (MI). We hypothesized that tissue necrosis is an activator of dendritic cells (DCs), which control tolerance to self-antigens. DC subsets of a murine healthy heart consisted of IRF8-dependent conventional (c)DC1, IRF4-dependent cDC2, and monocyte-derived DCs. In steady state, cardiac self-antigen α-myosin was presented in the heart-draining mediastinal lymph node (mLN) by cDC1s, driving the proliferation of antigen-specific CD4$^+$ TCR-M T cells and their differentiation into regulatory cells (Tregs). Following MI, all DC subsets infiltrated the heart, whereas only cDCs migrated to the mLN. Here, cDC2s induced TCR-M proliferation and differentiation into interleukin-(IL)-17/interferon-(IFN)γ-producing effector cells. Thus, cardiac-specific autoreactive T cells get activated by mature DCs following myocardial infarction.

INTRODUCTION

Autoreactive CD4$^+$ T cells are normally deleted during thymic negative selection, yet many self-reactive T cells escape this checkpoint, emerging as anergic, thymic regulatory (tTreg) or ignorant conventional T cells (Tconv) (Davis, 2015). Self-reactive T cell activation is a major culprit in autoimmune disease, and therefore tolerance to some tissue-restricted self-antigens is shaped entirely by extrathymic processes. Suppression of autoreactive CD4$^+$ T cells is dependent on peripheral dendritic cells (DCs), which present tissue-restricted self-antigens derived mostly from turnover of apoptotic cells (Steinman et al., 2003). In the absence of inflammation, self-antigen presentation by DCs results in T cell anergy, further expansion of tTregs, or generation of induced (i)Tregs from Tconv cells, thus promoting peripheral tolerance to the self-antigen (Ganguly et al., 2013). Lack of steady-state DCs results in loss of functional Tregs and subsequent activation of autoreactive Th1/Th17 effector cells, whereas increased numbers of immature DCs result in increased iTreg numbers, which prevent autoimmunity (Ohnmacht et al., 2009; Darrasse-Jèze et al., 2009). It is, however, equally important that DCs presenting self-antigen remain in a quiescent state, devoid of cytokine production that can break peripheral tolerance (Eriksson et al., 2003; Ardouin et al., 2016). Removal of inhibitory nuclear factor (NF)-κB signaling intermediates or artificial extension of DC life-span are sufficient to break self-tolerance (Kool et al., 2011; Stranges et al., 2007). Despite experiments clearly implicating DCs in the regulation of peripheral tolerance and induction of autoimmunity, the precise triggers that cause DC activation and possibly break self-tolerance are incompletely understood (Ganguly et al., 2013). Certain organ-directed infections trigger tissue-specific autoimmunity by promoting DC activation either through direct infection or release of cytokines that cause full DC maturation (Gangaplara et al., 2012; Torchinsky et al., 2009). Endogenous danger signals like uric acid or HMGB1 lead to DC maturation in response to sterile tissue injury (Scaffidi et al., 2002). Exposure of DCs to necrotic cells is sufficient to drive DC maturation in vitro (Gallucci et al., 1999). But currently, it is not known if sterile inflammation induced by tissue ischemia and necrosis causes DCs to drive the initiation of adaptive immune responses to self-antigen in vivo.

To address this, we chose a model of myocardial infarction (MI). Undoubtedly, tissue necrosis caused by coronary artery occlusion is one of the most common diseases of Western society, causing significant mortality and morbidity (Latet et al., 2015). MI results in necrotic cardiomyocytes releasing their intracellular contents, which act as danger signals that cause sterile inflammation (Zhang et al., 2015). In healthy mice and humans, CD4$^+$ T cells specific for cardiac self-antigen α-myosin heavy chain (αMyHC) escape thymic negative selection and seed the

periphery, rendering the heart vulnerable to an autoimmune attack (Lv et al., 2011). Up to 30% of MI patients develop signs of humoral autoimmunity that is often self-limiting but can be accompanied by pericarditis. This percentage increases to 80% of autoimmune prone type I diabetes (T1D) patients. Non-obese diabetic (NOD) mice, a mouse model of T1D, also develop pathologic cardiac autoimmunity post MI, whereas wild-type (WT) C57BL/6 mice do not (Gottumukkala et al., 2012; Lipes and Galderisi, 2015). Environmental cues from an infarcted heart are thus sufficient to induce heart-specific immunity in autoimmune prone hosts in the absence of microbial ligands. It was hypothesized before that the innate inflammatory response in the infarcted heart can initiate the maturation of DCs, licensing them for activation of T cells directed against the heart (Gottumukkala et al., 2012; Lv and Lipes, 2012); however, direct evidence of this DC-T cell interaction post MI is lacking. To study if danger signals released by tissue injury can activate DCs and generate adaptive immunity, TCR transgenic mice (TCR-M) have been developed to measure $CD4^+$ T cell responses to αMyHC (Nindl et al., 2012). Using these tools, we studied if, where, and how cardiac self-antigens are presented. In steady state, conventional type 1 DCs (cDC1s) presented cardiac self-antigen to αMyHC-specific TCR-M cells only in heart-draining mediastinal lymph nodes, leading to Treg expansion. In mice in which MI was induced, cardiac DCs were activated and in vivo αMyHC presentation was increased. Post MI, mainly conventional type 2 DCs (cDC2s) presented αMyHC and induced the formation of interferon (IFN)γ- and interleukin (IL)-17-producing TCR-M cells. These findings show that tissue necrosis activates autoreactive T cells through DC maturation and migration.

RESULTS

CD11c-Expressing Cells in the Heart Can Be Subdivided into cDC1s, cDC2s, and moDCs

Conventional DCs, which form the crucial link between innate and adaptive immunity, are divided into two subsets termed cDC1s and cDC2s (Guilliams et al., 2014). cDCs arise in a Flt3L-dependent manner from progenitors in the bone marrow (Waskow et al., 2008), and are divided based on surface markers and differential dependence on transcription factors (TFs) (Sichien et al., 2017). cDC1s express XCR1 and CD103 and depend on Batf3 and IRF8, whereas cDC2s express CD172α (SIRPα) and CD11b and partially depend on Zeb2 and IRF4 (Bajaña et al., 2012; Scott et al., 2016). Because DC subsets in the murine heart are poorly defined, we characterized subsets in the healthy heart. We used flow cytometry to identify $CD11c^+$ cells among live non-autofluorescent $CD45^+$ $Lineage^-$ cells. These were further divided based on MHCII and CD64 to identify $MHCII^+CD64^-$ cDCs and $CD64^+MHCII^+$ monocyte-derived DCs (moDCs) (Figure 1A). Embryonically derived macrophages (MFs) were outgated because these cells are autofluorescent and do not express CD11c (Molawi et al., 2014; Epelman et al., 2014). cDCs can be further subdivided into XCR-1^+ cDC1s and $CD172α^+$ cDC2s, whereas moDCs uniformly expressed CD172α. $CD11c^+$ cells made up 0.98% ± 0.27% (mean ± SEM) of all living heart cells and 7.39% ± 1.36% of $CD45^+$ leukocytes. cDC1s and cDC2s made up 4.77% ± 0.16% and 14.5% ± 1.25% of total CD11c-expressing cells, respectively, whereas 16.87% ± 3.09% of $CD11c^+$ cells were moDCs (Figures 1B and 1C). cDC development depends on Flt3L, whereas moDC development does not (Waskow et al., 2008). So to confirm cDC and moDC identification, hearts of $Flt3l^{-/-}$ mice were compared with $Flt3^{+/+}$ hearts. We found a severe reduction in cDC1s and cDC2s in the $Flt3l^{-/-}$ heart compared with WT mice, whereas moDCs were unaffected (Figures 1D and 1E), demonstrating that only heart cDCs are Flt3L dependent. We next examined the expression of surface markers associated with DC subsets (Figures 1F and 1G). Cardiac cDC subsets expressed the typical cDC markers CD26 (Miller et al., 2012) and Flt3. As described in other tissues, cDC2s and moDCs expressed CD11b, whereas cDC1s expressed CD103. cDC1s uniformly expressed CD24, whereas cDC2s were separated into $CD24^+$ and $CD24^-$ cDC2s, as described for lung cDC2s (Bajaña et al., 2016). Expression of CADM1, a universal cDC1 marker (Guilliams et al., 2016; Gurka et al., 2015), was restricted to cDC1s. MoDCs expressed the typical MF markers MerTK, Mar-1, and F4/80, although some F4/80 expression was also noted on cDC2s, as found in other tissues (Tamoutounour et al., 2013). As expected, moDCs expressed CCR2, which is critical for monocyte exit from the bone marrow. CCR2 was also expressed on cDCs, as observed in intestinal cDC2s (Scott et al., 2015).

We next FACS-purified cDC1s, cDC2s, moDCs, and $CD11c^-$ MFs from a steady-state heart and performed RNA-sequencing (RNA-seq) analysis (Figures 1H and 1I). To confirm identification of heart cDC1s and cDC2s, we generated a list of hallmark genes across a range of tissues by examining the transcriptomes of cDC subsets available from the Immgen consortium. Gene expression in cardiac APC populations was then studied. Cardiac cDC1s indeed expressed cDC1 genes, including *Clec9a*, *Cadm1*, *Itgae*, *Tlr3*, and *Irf8*, whereas these genes were lowly expressed by cardiac cDC2s, moDCs, and MFs (Figure 1H). cDC2 genes like *Cd11b*, *Cd72*, *Csf1r*, *Zeb2*, and *Irf4* were highly expressed by cardiac cDC2s compared with cDC1s (Figure 1I). Taken together, these data highlight the previously unappreciated heterogeneity among cardiac DCs.

Transcription Factor Dependency of Cardiac cDC Subsets

The molecular requirements for cardiac DC development have been poorly studied. Because cDC1s and cDC2s in other tissues are thought to depend on IRF8 and IRF4, respectively (Mildner and Jung, 2014), we hypothesized that this would be the same for cardiac cDCs. Therefore, we first examined IRF8 and IRF4 expression in cardiac DCs at the protein level (Figures 2A and 2B). IRF4 was most highly expressed by cardiac cDC2s, whereas cDC1s expressed high levels of IRF8. Next, we crossed mice expressing CRE recombinase under the control of the CD11c promoter (*Cd11cCre* mice) (Caton et al., 2007) with $Irf4^{flox}$ (Persson et al., 2013) or $Irf8^{flox}$ mice (Sichien et al., 2016) to generate mice lacking IRF4 or IRF8 expression, respectively, in $CD11c^+$ cells. Whenever CRE was expressed in $CD11c^+$ cells, *Irf4* or *Irf8* was efficiently floxed out and their protein levels declined (data not shown). Analysis of $Irf4^{fl/fl}$.*Cd11cCre* mice revealed that cardiac cDC2 ($CD172α^+CD24^{+/-}$) were only slightly reduced (Figures 2C and 2E). However, a significant reduction

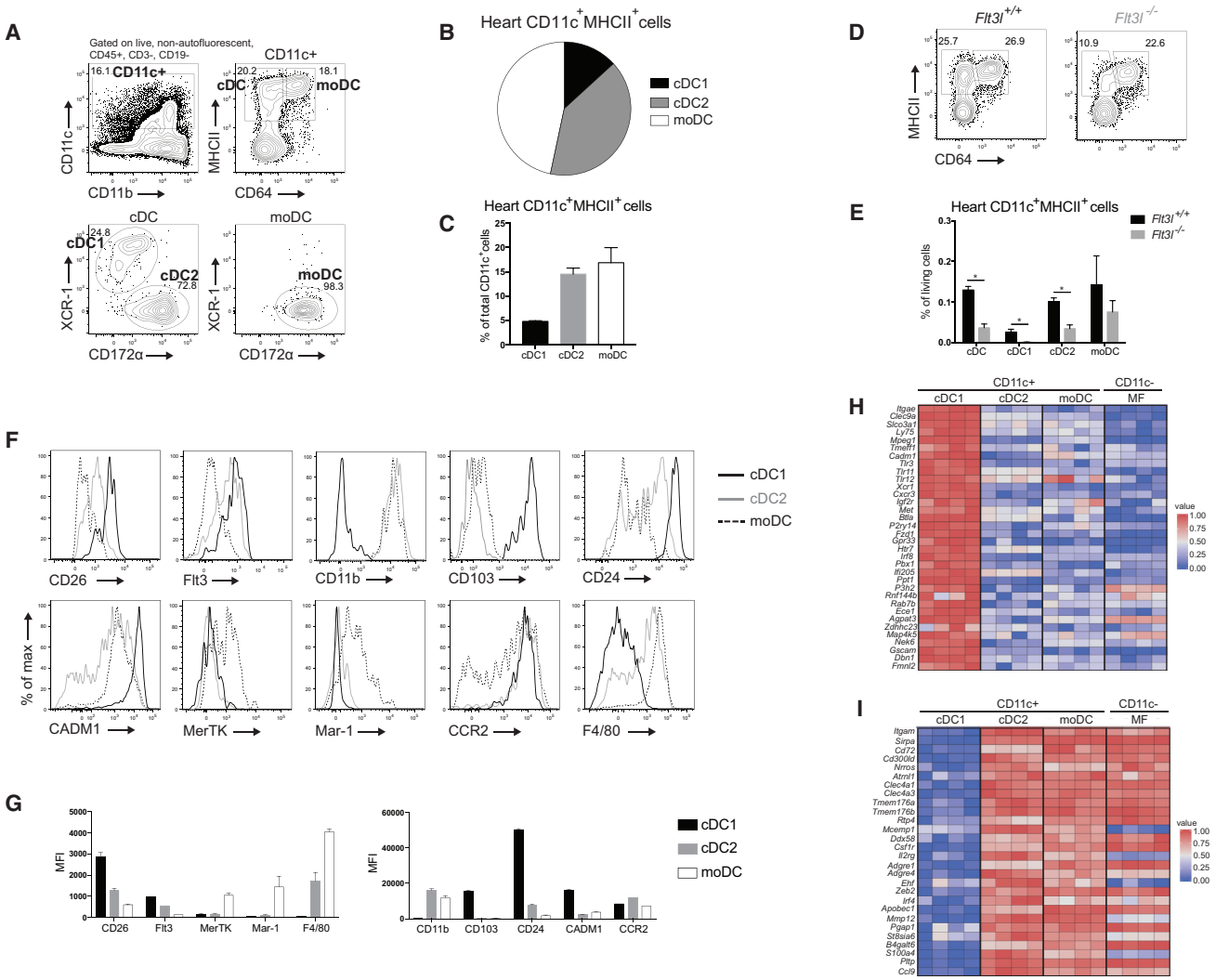

Figure 1. CD11c-Expressing Cells in the Heart Can Be Subdivided into cDC1s, cDC2s, and moDCs

(A) Flow cytometry gating strategy for DC subsets in steady-state heart of WT mice.

(B) Pie chart representing the distribution of DC subsets in naive murine WT heart.

(C) DC subset percentages of total CD11c$^+$ cells in naive heart of WT mice.

(D) Expression of MHCII and CD64 in CD45$^+$Lineage$^-$CD11c$^+$ cells from naive heart in *Flt3l*$^{+/+}$ and *Flt3l*$^{-/-}$ mice.

(E) Total cDC, cDC1, cDC2, and moDC percentages of total living cells in naive heart of *Flt3l*$^{+/+}$ and *Fltl3*$^{-/-}$ mice.

(F) Representative histograms of CD26, Flt3, CD11b, CD103, CD24, CADM1, MerTK, Mar-1, CCR2, and F4/80 expression in steady-state WT heart cDC1s, cDC2s, and moDCs (n = 3).

(G) MFI of marker expression on steady-state WT heart DC subsets shown in (F).

(H and I) Heat map of relative expression of (H) hallmark cDC1 genes and (I) hallmark cDC2 genes in cDC1s, cDC2s, moDCs, and MFs sorted from naive WT hearts acquired by RNA-seq. All data in Figure 1 represent at least two independent experiments, and all bar graphs show data as mean ± SEM (*p ≤ 0.05).

in CD24$^+$ cDC2s was observed, suggesting that IRF4 is important for their terminal differentiation, as described in the lung (Bajaña et al., 2016). Because IRF4 has also been implicated in regulating cDC2 migration (Bajaña et al., 2012), we next studied cDC2 frequency in the heart-draining mediastinal lymph node (mLN) (Figures 2D and 2E). Migration of both CD24$^+$ and CD24$^-$ cDC2s was indeed lower in the mLN of *Irf4*$^{fl/fl}$*.Cd11cCre* mice. Examination of cDC subsets in the heart and mLN of *Irf8*$^{fl/fl}$*.Cd11cCre* mice demonstrated an almost complete ablation of cDC1s (CD24$^+$CD172α^-) in both locations (Figures 2F–2H). cDC2s were unaffected in the *Irf8*$^{fl/fl}$*.Cd11cCre* heart, but were significantly increased in the mLN. Thus, cardiac cDC1s and cDC2s, similarly to their counterparts in other organs, depend on IRF8 and IRF4, respectively, for their development (cDC1s and CD24$^+$ cDC2s) and migration to the lymph nodes (LNs) (cDC2s). Thus, *Irf8*$^{fl/fl}$*.Cd11cCre* and *Irf4*$^{fl/fl}$*.Cd11cCre* mice represent two models in which cardiac cDC1 and cDC2 function, respectively, can be assessed.

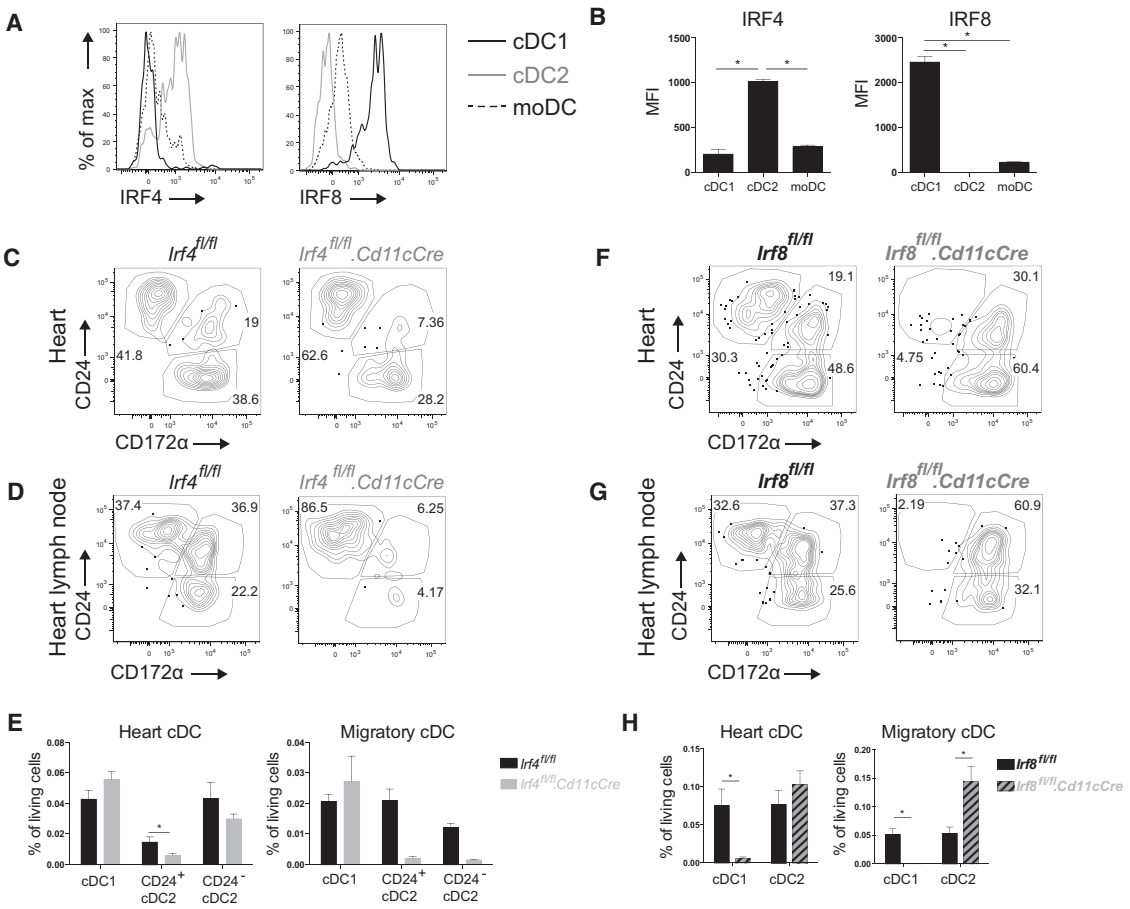

Figure 2. Transcription Factor Dependency of Cardiac cDC Subsets

(A) Representative histogram of IRF4 and IRF8 expression of steady-state WT heart cDC1s, cDC2s, and moDCs.

(B) MFI of IRF4 and IRF8 expression on naive WT heart DC subsets shown in (A).

(C and D) MHCII$^+$CD11c$^+$CD64$^-$ cDCs are divided into CD24$^+$CD172α^- cDC1s, CD24$^+$CD172α^+ cDC2s, and CD24$^-$CD172α^+ cDC2s in *Irf4*$^{fl/fl}$ and *Irf4*$^{fl/fl}$*.Cd11cCre* steady-state heart (C) and mediastinal LN (D).

(E) Percentage of living cells of cDCs in *Irf4*$^{fl/fl}$ and *Irf4*$^{fl/fl}$*.Cd11cCre* naive heart and mLN.

(F and G) MHCII$^+$CD11c$^+$CD64$^-$ cDCs are divided into CD24$^+$CD172α^- cDC1s, CD24$^+$CD172α^+ cDC2s, and CD24$^-$CD172α^+ cDC2s in *Irf8*$^{fl/fl}$ and *Irf8*$^{fl/fl}$*.Cd11cCre* steady-state heart (F) and mLN (G).

(H) Percentage of living cells of cDCs in *Irf8*$^{fl/fl}$ and *Irf8*$^{fl/fl}$*.Cd11cCre* steady-state heart and mLN. All data in Figure 2 represent at least two independent experiments, and all bar graphs show data as mean ± SEM (*p ≤ 0.05).

IRF8-Dependent cDC1s Generate Myosin-Specific Tregs in Heart-Draining Lymph Node

Although the heart is not continuously exposed to environmental antigens compared with mucosal surfaces, heart DCs can encounter cardiac self-antigens, such as α-myosin heavy chain (αMyHC). Because αMyHC autoreactive CD4$^+$ T cells escape from the thymus into the periphery (Lv et al., 2011), it is plausible that cardiac DCs would function in preserving peripheral tolerance to the heart. Thus, we next examined if cardiac cDC1s or cDC2s played such a role. A critical tool to answer this key question was αMyHC-specific TCR-M mice (Nindl et al., 2012). Naive CD62L$^+$CD44$^-$ CD4$^+$ T cells were purified from TCR-M splenocytes, CFSE labeled, and injected into steady-state WT littermates (*Irf4*$^{fl/fl}$ *and Irf8*$^{fl/fl}$ mice without *Cd11cCre* expression) to determine if and where αMyHC is presented. Various lymphoid organs of acceptor mice were collected for analysis 3 days after TCR-M transfer. Undivided TCR-M cells were present in all organs examined, consistent with the migratory behavior of naive T cells (Figures 3A and 3D). TCR-M proliferation detected by CFSE dilution and CD44 expression was exclusively observed in the heart-draining mediastinal LN of naive WT mice. TCR-M proliferation and activation in mLN demonstrated αMyHC transport and presentation without the presence of cardiac damage (Figures 3B and 3E). Upon division, TCR-M cells gained expression of T-bet and RoRγt, respectively, and TFs for Th1 and Th17 cells (Figures 3C and 3F). Divided cells also expressed Foxp3 and CD25 indicative for Tregs (Figures 3C and 3F). To verify if migratory cDC2s were responsible for αMyHC presentation in mLN, naive TCR-M cells were injected in *Irf4*$^{fl/fl}$*.Cd11cCre* mice. TCR-M cells in *Irf4*$^{fl/fl}$*.Cd11cCre* mLN proliferated equally well as in WT littermates, indicating that cDC2 migration is not necessary for αMyHC presentation (Figures 3A and 3B). T-bet,

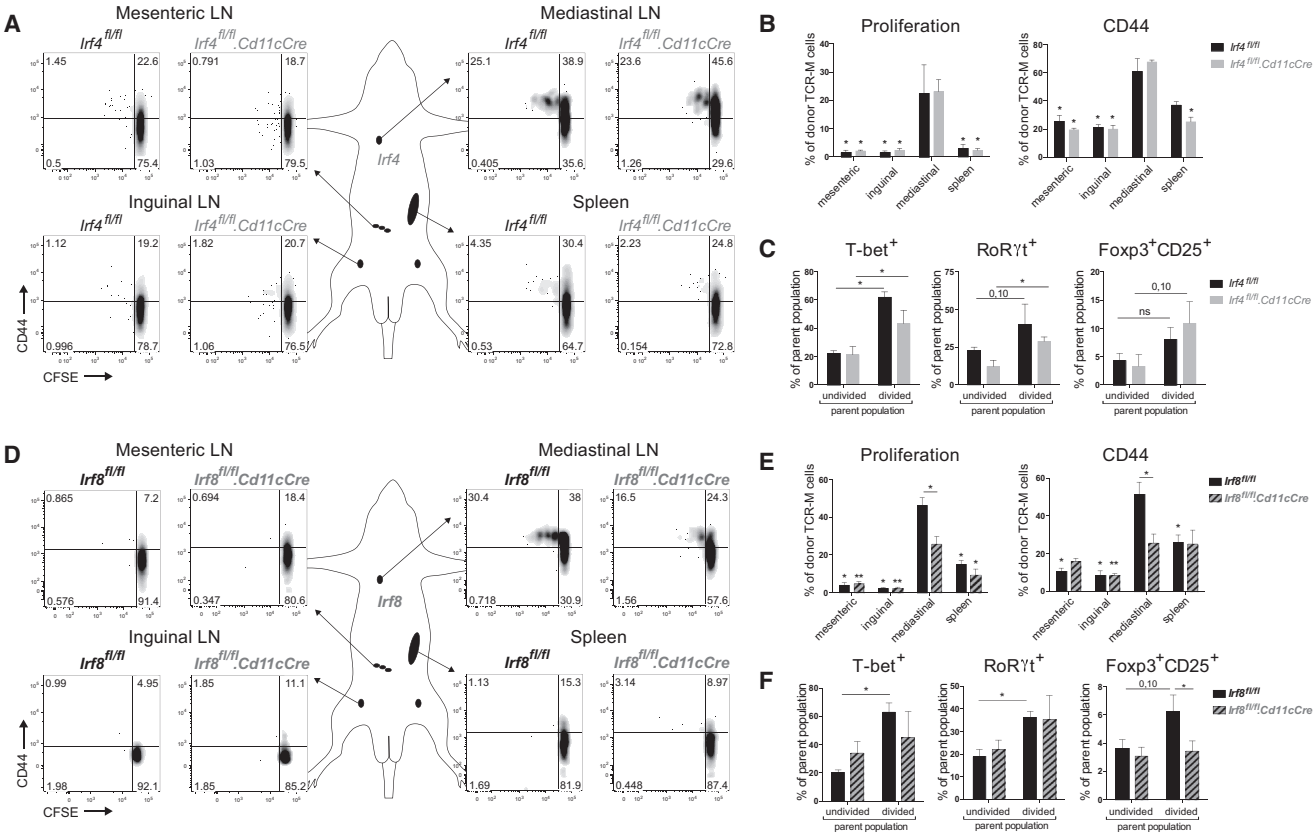

Figure 3. IRF8-Dependent cDC1s Generate Myosin-Specific Tregs in Heart-Draining Lymph Node

(A) Depicted LNs and spleen were isolated from TCR-M acceptor *Irf4*$^{fl/fl}$ and *Irf4*$^{fl/fl}$*.Cd11cCre* mice 3 days after naive TCR-M transfer. CFSE dilution and CD44 expression of donor TCR-M cells was analyzed by flow cytometry.

(B) Percentage of proliferation and CD44 expression of donor TCR-M cells in LNs and spleen from the experiment described in (A) (n = 4).

(C) Percentage of T-bet, RoRγt, and Foxp3/CD25 expression on undivided and divided donor TCR-M cells isolated from mLN in *Irf4*$^{fl/fl}$ and *Irf4*$^{fl/fl}$*.Cd11cCre* steady-state mice (n = 4).

(D) 3 days after naive TCR-M injection, depicted LNs and spleen were isolated from TCR-M acceptor *Irf8*$^{fl/fl}$ and *Irf8*$^{fl/fl}$*.Cd11cCre* mice. CFSE dilution and CD44 expression of donor TCR-M cells was analyzed by flow cytometry.

(E) Percentage of proliferation and CD44 expression of donor TCR-M cells in LNs and spleen from the experiment described in (D) (n = 5).

(F) Percentage of T-bet, RoRγt, and Foxp3/CD25 expression on undivided and divided donor TCR-M cells isolated from mLN in *Irf8*$^{fl/fl}$ and *Irf8*$^{fl/fl}$*.Cd11cCre* steady-state mice (n = 5). All data in Figure 3 represent at least three independent experiments, and bar graphs show data as mean ± SEM (*p ≤ 0.05).

RoRγt, and Foxp3 increase upon division was unchanged in *Irf4*$^{fl/fl}$*.Cd11cCre* mLN compared with *Irf4*$^{fl/fl}$ (Figure 3C). Naive TCR-M cells were next administered to *Irf8*$^{fl/fl}$*.Cd11cCre* mice to study if cDC1s were responsible for steady-state αMyHC presentation. Proliferation and CD44 expression was significantly lower in mLN of *Irf8*$^{fl/fl}$*.Cd11cCre* mice compared with *Irf8*$^{fl/fl}$ mice 3 days post-transfer (Figures 3D and 3E). Although T-bet and RoRγt upregulation in divided TCR-M cells was not altered in *Irf8*$^{fl/fl}$*.Cd11cCre* mLN (Figure 3F), Foxp3 induction was significantly reduced in divided TCR-M cells from *Irf8*$^{fl/fl}$*.Cd11cCre* mLN, showing a block in iTreg generation in the absence of cDC1s. Our findings identify cardiac cDC1s as necessary for αMyHC-specific Treg induction from naive TCR-M cells.

DCs Infiltrate the Heart and Migrate to the Mediastinal Lymph Node Following MI

MI triggers an inflammatory response characterized by infiltration of innate immune cells (Latet et al., 2015). Although infiltration of DCs has been described in infarcted hearts (Maekawa et al., 2009), DC subsets have not been identified. Thus, we first sought to characterize DC subsets post MI. We induced MI in WT female mice by permanently ligating the left anterior descending (LAD) coronary artery and examined DCs at various time points post-surgery. Consistent with previous reports, the proportion of CD11c$^+$ cells was increased compared with sham-operated controls (Figure 4A). A significant part of CD11c$^+$ cells in MI hearts was CD64$^+$MHCII$^-$. These cells were not further analyzed because they lacked MHCII expression. They are probably MFs recruited due to MI, as seen in other sterile inflammation models (Zigmond et al., 2014). At day 7 post-surgery, we also observed a dramatic increase in moDCs (CD64$^+$CD172α$^+$) in MI hearts compared to sham (Figures 4A and 4B). Analysis of DC subsets between 2 and 10 days post MI revealed an increase of all subsets by day 2 post MI, with the peak of XCR-1$^+$ cDC1 and moDC infiltration at day 7. CD172α$^+$ cDC2 numbers peaked at day 5 post MI. moDCs contributed most to the total infarcted heart

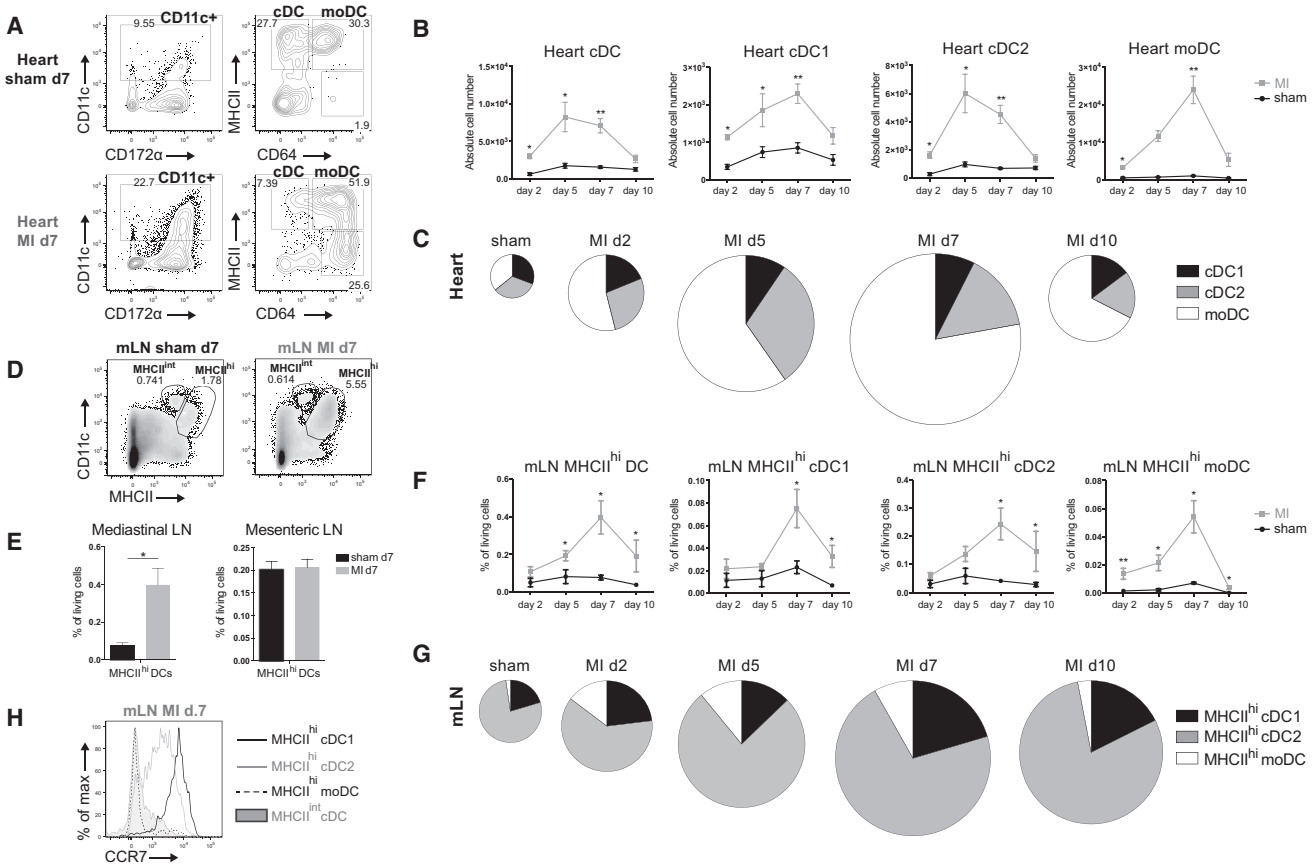

Figure 4. DCs Infiltrate the Heart and Migrate to Mediastinal Nodes Following MI

(A) Representative gating strategy for DC subsets in the heart of sham-operated and infarcted WT mice on day 7 post-surgery.

(B) Absolute cell numbers of DC subsets in the heart of sham-operated and infarcted mice on day 2, 5, 7, and 10 post-surgery (n = 3–6).

(C) Pie charts depicting the distribution of DC subsets in the sham-operated heart (pooled data from day 2-5-7-10 post-surgery) and infarcted heart on day 2, 5, 7, and 10 post-MI. Pie chart sizes are proportional to total cardiac DC percentages.

(D) Representative gating strategy for MHCII^{int} and MHCII^{hi} DCs in mediastinal LN of sham-operated and infarcted WT mice on day 7 post-surgery.

(E) MHCII^{hi} DC percentages of total living cells in mediastinal and mesenteric LN in sham-operated and infarcted mice at day 7 post-surgery (n = 6).

(F) MHCII^{hi} DC subset percentages of total living cells in mediastinal LN of sham-operated and infarcted mice on day 2, 5, 7, and 10 post-surgery (n = 3–6).

(G) Pie chart illustrating distribution of cDC1s, cDC2s, and moDCs among total MHCII^{hi} DC population in mLN in sham-operated and infarcted mice at day 2, 5, 7, and 10 post-surgery. Pie chart sizes are proportional to total MHCII^{hi} DCs in mLN.

(H) Representative histogram of CCR7 expression of MHCII^{hi} cDC1s, MHCII^{hi} cDC2s, MHCII^{hi} moDCs, and MHCII^{int} cDCs from mLN on day 7. All bar graphs in Figure 4 show data as mean ± SEM (*p ≤ 0.05; **p ≤ 0.01), and all data are representative of two independent experiments.

DC population. All subsets returned to near baseline levels within 10 days (Figures 4B and 4C). Next, we studied migration to the heart-draining mediastinal LN post MI. Typically, DCs that have migrated to the LN from the periphery are MHCII^{hi}, in contrast to LN-resident DCs that are MHCII^{int}. An increase in MHCII^{hi} DCs was observed in mediastinal, but not mesenteric, LNs 7 days post MI compared with sham (Figures 4D and 4E). Among MHCII^{hi} DCs, we identified XCR-1^{+} cDC1s, CD172α^{+} cDC2s, and CD64^{+} moDCs. We followed DC migration to the mediastinal LN between 2 and 10 days post-surgery (Figures 4F and 4G). Consistent with heart DC infiltration, MHCII^{hi} DC subsets peaked at day 7 post MI. MHCII^{hi} cDC2s represented the largest DC population. To validate if DCs had indeed migrated from the heart, we examined CCR7 expression, the chemokine receptor required for migration to the LN (Ohl et al., 2004). As expected, MHCII^{hi} cDC1s and cDC2s expressed CCR7 and hence migrated to the LN, whereas MHCII^{int} cDCs lacked CCR7 (Figure 4H). However, MHCII^{hi} moDCs did not express CCR7, suggesting that moDCs have not migrated from the heart and instead have merely upregulated MHCII, as has been reported (Tamoutounour et al., 2013).

DCs from Infarcted Heart Have an Activated Phenotype

To gain more insight in the phenotype of DCs infiltrating the infarcted heart, we performed RNA-seq on heart cDC1s, cDC2s, and moDCs sorted from post MI day 7 hearts. As a reference population, we also sorted cardiac CD11c^{-} MFs (Lineage^{-}CD11c^{-}MHCII^{+}CD64^{+}CD172α^{+}). Unsupervised principle-component analysis (PCA) showed that irrespective of the heart tissue environment (steady state or MI), cardiac DCs clustered

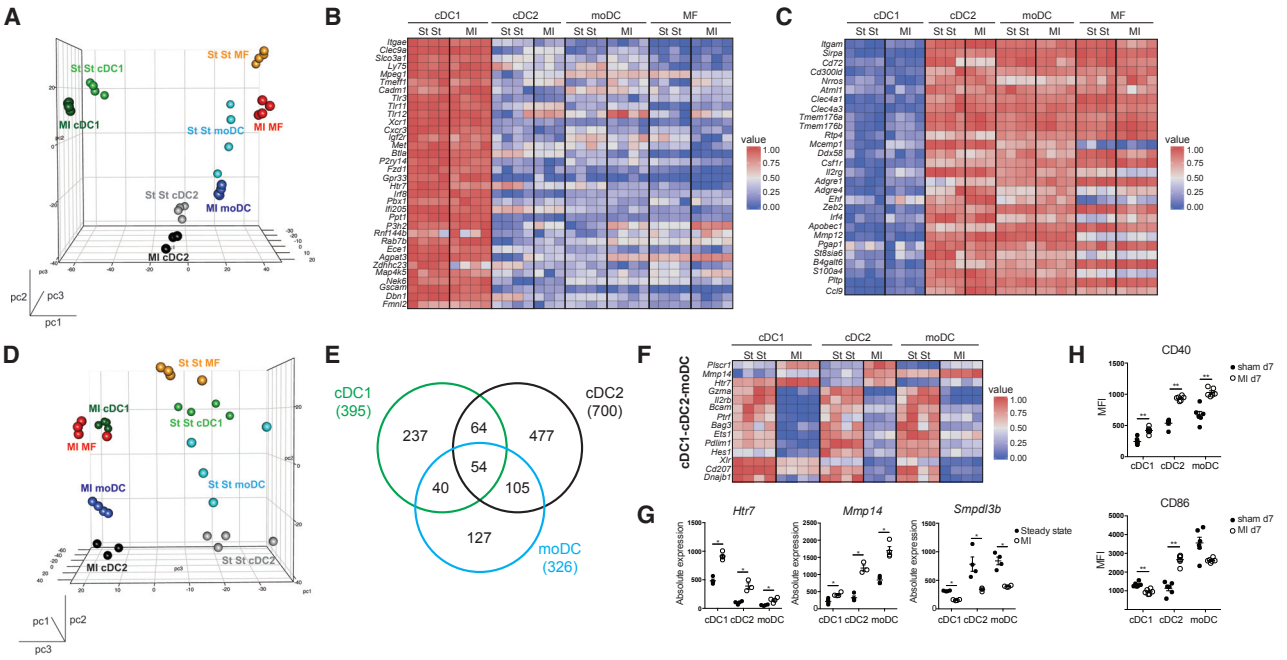

Figure 5. DCs from Infarcted Heart Have an Activated Phenotype

(A) Front view of PCA of RNA-seq data from cDC1s, cDC2s, moDCs, and MFs in the steady-state (St St) and the infarcted (MI d7) heart. PCA was calculated using the top 15% most varying genes between cell subsets. Each dot symbolizes one independently sorted replicate of the indicated cell population, and four independent sorts were performed per subset.

(B and C) Heat map of relative expression of hallmark cDC1 genes (B) and hallmark cDC2 genes (C) in cDC1s, cDC2s, moDCs, and MFs sorted from steady-state and infarcted hearts.

(D) Side view of PCA of RNA-seq data from cDC1s, cDC2s, moDCs, and MFs in the steady-state and infarcted heart.

(E) Venn diagram showing numbers and overlap of DEGs in cDC1s, cDC2s, and moDCs sorted from MI d7 compared to steady-state hearts.

(F) Heat map of relative expression of top-shared DEGs between DC subsets from MI d7 hearts compared to corresponding subsets isolated from the steady-state heart. To calculate top DEGs, a threshold of a minimum 1.5 Log2 fold change was used. As an exception, no threshold was set on shared upregulated genes of cDC1s, cDC2s, and moDCs.

(G) Bar graphs representing absolute expression of DEGs among cDC1s, cDC2s, and moDCs sorted from steady-state and infarcted hearts.

(H) MFI of CD40 and CD86 expression (day 7 post-surgery) on heart DC subsets in sham-operated compared to the infarcted heart (n = 6). All bar graphs in Figure 5 show data as mean ± SEM (*$p \leq 0.05$; **$p \leq 0.01$), and all data are representative of four independent experiments.

See also Figure S1 and Tables S1–S7.

by subset on principal components 1 (pc1) and 2 (pc2) (Figure 5A). Also, expression of hallmark cDC1 (Figure 5B) and cDC2 genes (Figure 5C) did not change in cardiac DCs post MI. Interestingly, pc3 divided cell subsets into two groups, those deriving from the steady state or infarcted heart (Figure 5D), suggesting a global MI signature, which was conferred upon the subsets post MI. To further examine the MI signature, gene expression of infarcted heart DCs was compared with that of steady-state heart DCs to identify differentially expressed genes (DEGs). We found that 395, 700, and 326 genes were differentially expressed in cDC1s, cDC2s, and moDCs, respectively, between healthy and infarcted hearts (Figure 5E; Tables S1–S3). To determine the global MI signature, we assessed which DEGs were conserved between DC subsets and found that 54 genes were differentially expressed in the three DC subsets (Figures 5E and 5F; Table S4). Analysis of these 54 genes suggested that DC subsets would be altered in their activation status. *Htr7* (encoding serotonin receptor 5-HT_7R) and *Mmp14* (encoding metalloproteinase MMP-14) were both upregulated in MI and are linked to DC migration (Figures 5F and 5G; complete DEG lists can be found in the Supplemental Information; Tables S5–S7) (Holst et al., 2015; Gawden-Bone et al., 2010). *Smpdl3b* (encoding sphingomyelin phosphodiesterase, acid-like 3B) was downregulated and encodes a negative regulator of TLR signaling (Heinz et al., 2015), suggesting increased TLR signaling in post MI DCs. Recently, several gene clusters were found to be induced upon homeostatic or TLR-induced cDC1 maturation (Ardouin et al., 2016). We observed that cDC1s from MI hearts were enriched for genes upregulated by TLR-induced maturation, suggesting that cDC1s in infarcted hearts were indeed induced to mature in a TLR-dependent manner (Figures S1A and S1D). cDC2s and moDCs from MI hearts were enriched in genes upregulated by TLR-induced and homeostatic maturation (Figures S1B S1D).

To determine if DCs were also activated at the protein level post MI, expression of the activation markers CD40 and CD86 was examined by flow cytometry during the peak of DC infiltration (day 7). As predicted by RNA-seq, the ischemic environment induced DC activation. All DC subsets showed increased expression of CD40 post MI (Figure 5H). However, CD86 expression was only increased on cDC2s from infarcted hearts.

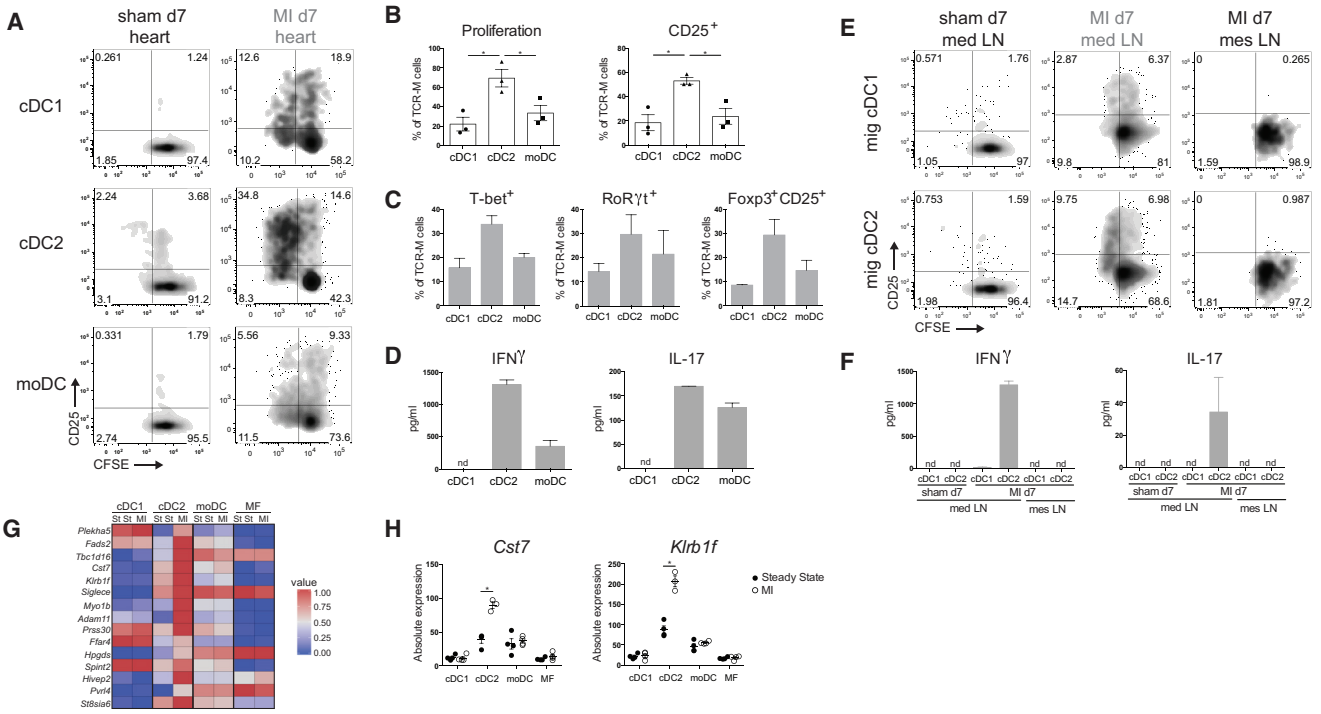

Figure 6. cDC2s Are the Main Presenters of αMyHC to Effector Autoreactive CD4+ T Cells Ex Vivo

(A) CFSE dilution and CD25 expression of TCR-M cells in co-culture with sorted heart DC subsets from sham-operated versus MI d7 mice. Data are representative of three independent experiments (n = 12).

(B) Quantification of percentages of proliferated and CD25-expressing TCR-M cells from co-cultures plotted in (A). Individual dots represent the value of one independent experiment (mean ± SEM; *p ≤ 0.05).

(C) Percentage of T-bet, RoRγt, and Foxp3/CD25 expression on TCR-M cells co-cultured with sorted heart DC subsets from MI day 7 hearts (mean ± SEM).

(D) In supernatants of co-cultures plotted in (A), cytokines produced by TCR-M cells were detected by ELISA. Mean is calculated from values of technical replicates from one experiment (nd, not detectable) (mean ± SD).

(E) CFSE dilution and CD25 expression of TCR-M cells co-cultured with sorted migratory cDC1s and cDC2s from mLNs of sham-operated and MI mice and from mesenteric LNs of MI mice.

(F) After 3 days of co-culture (plotted in E), cytokines were measured in supernatants by ELISA. Mean is calculated from values of technical replicates from one experiment (nd, not detectable) (mean ± SD).

(G) Heat map of relative expression of cDC2 genes exclusively upregulated in cDC2s from the infarcted heart compared to steady state.

(H) Bar graphs representing absolute expression of interesting unique cDC2 DEGs (mean ± SEM; *p ≤ 0.05).

See also Table S8.

cDC2s Are the Main Presenters of αMyHC to Effector Autoreactive CD4+ T Cells Ex Vivo

Having shown that DCs infiltrate the heart, adopt an activated phenotype post MI, and migrate to mLN, we next examined if they presented the cardiac self-antigen αMyHC, released from necrotic cardiomyocytes to autoreactive T cells. To this end, we sorted cDC1s, cDC2s, and moDCs from the heart at day 7 post MI and sham controls and co-cultured them ex vivo with TCR-M cells. Consistent with cDC2s being superior at presenting antigen to CD4+ T cells and with their mature state post MI, proliferation and activation of TCR-M cells was increased when co-cultured with cDC2s from MI hearts compared with cDC1s and moDCs (Figures 6A and 6B). Nonetheless, cDC1s and moDCs from the MI heart induced more TCR-M proliferation compared to subsets from the sham heart (Figure 6A). Fitting with the highest proliferation, TCR-M cells cultured with heart cDC2s post MI exhibited increased expression of T-bet, RoRγt, and Foxp3 (Figure 6C) and the highest IFNγ and IL-17 production (Figure 6D). Migratory cDC2s sorted from mLN 7 days post MI were similarly best at inducing TCR-M proliferation, whereas migratory cDC1s only activated TCR-M cells (Figures 6E and 6F). Importantly, neither migratory cDCs from sham mLN nor migratory cDCs from mesenteric LN post MI stimulated TCR-M cells. To look further into the mechanisms of cDC2 superiority, we returned to our RNA-seq analysis. Using a stringent cut off described in the Supplemental Experimental Procedures, the list of cDC2 DEGs (MI compared to steady state) was reduced from 477 to 31 (Table S8). 15 DEGs were upregulated (Figure 6G), including *Cst7* (encoding cystatin F) and *Klrb1f* (encoding killer cell lectin-like receptor subfamily B member 1F) (Figure 6H), which encode proteins involved in antigen processing on MHCII (Magister et al., 2012) and T cell stimulation, respectively (Tian et al., 2005). This provides a plausible mechanism for the increased ability of cDC2s from the infarcted heart to present αMyHC to TCR-M cells.

Myocardial Infarction Activates Autoreactive CD4$^+$ T Cells In Vivo

Having shown that MI induces cardiac self-antigen presentation by DCs ex vivo, we next sought to examine if MI would activate autoreactive T cells in vivo. Therefore, naive TCR-M cells were transferred to MI and sham mice 2 and 7 days post-surgery and proliferation was analyzed 3 days later. TCR-M proliferation was increased in mLN of mice injected at day 2 post MI compared with sham, in vivo demonstrating increased αMyHC presentation early post MI (Figures 7A and 7B). TCR-M cells transferred to mice at day 2 post MI did not upregulate CD25 and Foxp3 Treg markers in mLN compared to sham mLN (Figure 7C). This suggests that iTreg differentiation was blunted after MI, potentially leading to a break in self-tolerance to the heart. Remarkably, TCR-M cells also proliferated in non-heart-draining lymphoid organs like the spleen and mesenteric LNs of MI mice compared with sham at day 2 (Figures 7A and 7B). This could suggest early systemic release of αMyHC post MI, which is presented by cDCs in non-draining lymphoid organs. Alternatively, divided TCR-M cells in non-draining LNs could be recirculating TCR-M cells that originally divided in mLN. To address this, an ex vivo co-culture was set up with bulk LN cells from sham d2, MI d2, and MI d7 mice as the antigen source and naive TCR-M cells as the readout for antigen presence (Figure 7D). TCR-M cells exclusively proliferated in the presence of mLN cells from MI d2 and d7 mice and not with mesenteric LN and spleen cells, suggesting that αMyHC is not systemically released in sufficiently high amounts post MI to stimulate TCR-M cells in this in vitro setting.

Presentation of Cardiac Myosin in the Absence of cDC Subsets following MI

Having demonstrated that self-antigen is presented to autoreactive T cells both ex vivo and in vivo, with cDC2s appearing to be specialized in this, we next set out to determine which cDC subsets were necessary and/or sufficient for presenting αMyHC post MI. We opted to use *Irf4*$^{fl/fl}$*.Cd11cCre* and *Irf8*$^{fl/fl}$*.Cd11cCre* mice. Although loss of IRF4 did not decrease cDC2 populations in the sham and MI heart, migratory cDC2s in the mLNs were significantly reduced (Figure 7E); thus, these mice could be used to assess the role of migratory cDC2s post MI. Naive TCR-M cells were then transferred to *Irf4*$^{fl/fl}$*.Cd11cCre* mice 2 days post MI. Intriguingly, decrease in migratory cDC2s in mLN of *Irf4*$^{fl/fl}$*.Cd11cCre* mice did not affect TCR-M proliferation and activation compared with *Irf4*$^{fl/fl}$ mice (Figures 7F and 7G), demonstrating that cDC2s are not necessary. To examine if cDC1s are needed, we performed the same experiment in *Irf8*$^{fl/fl}$*.Cd11cCre* mice because they lack cDC1s in the heart and mLN in both sham and MI mice (Figure 7H and data not shown). cDC1 loss had little effect on TCR-M proliferation and activation (Figure 7I). Proliferation was slightly reduced compared with *Irf8*$^{fl/fl}$ controls but was still ~80%. So neither cDC1s nor cDC2s are specifically required for the presentation of αMyHC to autoreactive CD4$^+$ T cells post MI.

DISCUSSION

It is widely accepted that DCs play a role in both the regulation of peripheral tolerance and induction of autoimmunity. However, the exact mechanisms that cause DC activation and hence break tolerance remain to be dissected. One proposed mechanism is the maturation of DCs by necrotic cells (Gallucci et al., 1999); however, because this study was performed in vitro, it remains unclear if and how tissue necrosis would contribute to the initiation of autoimmunity in vivo. In this study, we addressed this issue using MI as a model of tissue necrosis. Intracellular contents released from necrotic cardiomyocytes can behave like danger signals, resulting in a sterile inflammatory response (Zhang et al., 2015). Prior to profiling the effects of MI on cardiac DCs, we performed a comprehensive analysis of distinct DC populations during homeostasis. Similar to other tissues, the steady-state heart contains a population of CD11c$^+$MHCII$^+$ cells, which we termed DCs. Further analysis led us to conclude that heart DCs could be divided into two populations of conventional DCs, termed cDC1s and cDC2s (Guilliams et al., 2014), and a population CD64$^+$CD11c$^+$MHCII$^+$, which we termed moDCs, in line with what these cells were called previously (Tamoutounour et al., 2013). There is considerable controversy surrounding the correct name for this latter population because it is unclear if they are a bona fide DC population or a type of macrophage (Guilliams et al., 2016; Wu et al., 2016). Indeed, moDCs did not migrate from the heart to the LN, a hallmark of genuine DCs. However, moDCs did induce CD4$^+$ T cell proliferation in ex vivo co-cultures to the same extent as cDC1s and higher than CD11c$^-$ MFs (data not shown). Principal component analysis of gene expression also demonstrated that moDCs segregate in between cDCs and MFs. Thus, the exact nature and nomenclature of these cells remains unclear.

Because αMyHC-specific autoreactive CD4$^+$ T cells escape the thymus, peripheral tolerance is essential to prevent a cardiac autoimmune attack (Lv et al., 2011). Although cardiac DCs have been proposed to play a role in self-tolerance (Hart and Fabre, 1981), migration of self-antigen-loaded DCs to the draining LN had not been experimentally verified. Here, we demonstrated that naive αMyHC-reactive TCR-M cells proliferated in the heart-draining mLN without inducing cardiac damage and that they partially adopted an iTreg phenotype. It has recently been shown that cDC1s and cDC2s can induce iTregs in mesenteric LNs, with redundancy observed in mice lacking either cDC1s or cDC2s (Esterházy et al., 2016). Accordingly, while observing a reduction in iTreg generation in mLNs of steady-state *Irf8*$^{fl/fl}$*.Cd11cCre* mice, the lack of cDC1s did not disrupt cardiac tolerance (unpublished data). We speculate that there is some redundancy among cardiac cDC subsets, which prevents autoimmunity in the absence of cDC1s.

Consistent with studies examining all DCs (Anzai et al., 2012; Zhang et al., 1993), we observed a significant yet transient increase in cardiac DC subsets post MI. RNA-seq analysis revealed that although heart cDC subsets retained their hallmark genes, the ischemic environment induced some changes compared with steady-state DCs. Analysis of DEGs identified a core MI signature, proposing that DCs from the infarcted heart had a more activated phenotype. Analysis of maturation markers confirmed this at the protein level. This is consistent with reports demonstrating that necrotic cardiomyocytes release danger signals, including Hsp70 (Maekawa et al., 2009), interleukin-1α, and HMGB-1 (Zhang et al., 2015), which can promote DC activation

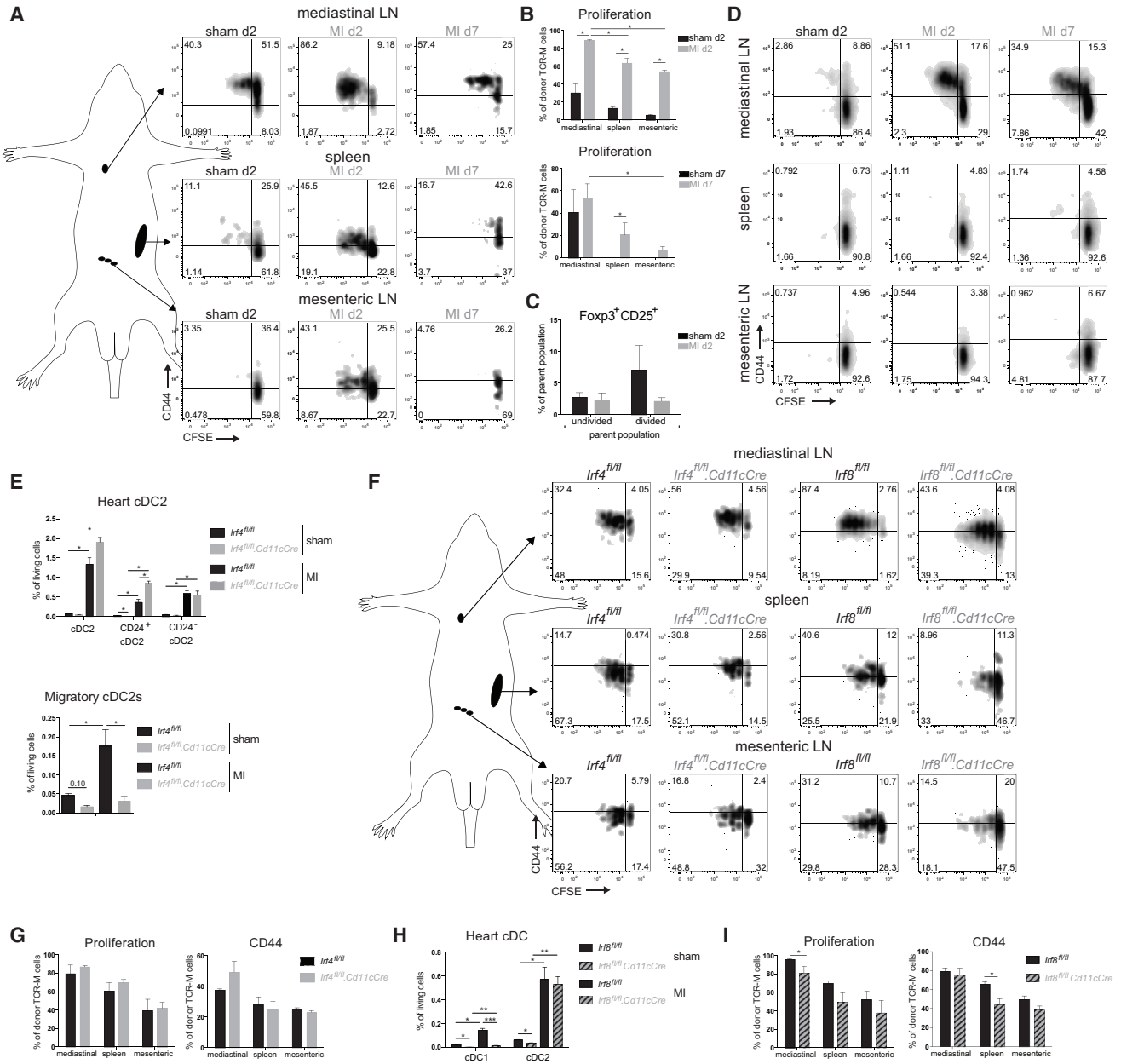

Figure 7. Myocardial Infarction Activates Autoreactive CD4⁺ T Cells In Vivo

(A) TCR-M cells were injected into sham or MI mice on day 2 or day 7 post-surgery. CFSE dilution and CD44 expression of donor TCR-M cells is shown.

(B) Proliferation of donor TCR-M cells in lymphoid organs from the experiment described in (A).

(C) Percentage of Foxp3/CD25 expression on undivided and divided donor TCR-M cells isolated from mLN in sham and MI mice at day 2 post-surgery.

(D) CFSE dilution and CD44 expression of naive TCR-M cells in ex vivo co-culture with bulk mediastinal LN, spleen, and mesenteric LN cells isolated from sham and MI mice on day 2 and day 7 post-surgery.

(E) Heart cDC2 and migratory cDC2 percentages in mLN of sham and MI *Irf4*$^{fl/fl}$ and *Irf4*$^{fl/fl}$.*Cd11cCre* mice at day 7 post-surgery.

(F) *Irf4*$^{fl/fl}$, *Irf4*$^{fl/fl}$.*Cd11cCre*, *Irf8*$^{fl/fl}$ and *Irf8*$^{fl/fl}$.*Cd11cCre* mice were injected with TCR-M cells at day 2 post MI. CFSE dilution and CD44 expression of donor TCR-M cells is shown.

(G) Proliferation and CD44 expression of donor TCR-M cells in LNs and spleen from *Irf4*$^{fl/fl}$ and *Irf4*$^{fl/fl}$.*Cd11cCre* mice from the experiment described in (F).

(H) Heart cDC percentages of sham and MI *Irf8*$^{fl/fl}$ and *Irf8*$^{fl/fl}$.*Cd11cCre* mice at day 7 post-surgery.

(I) Proliferation and CD44 expression of donor TCR-M cells in LNs and spleen from *Irf8*$^{fl/fl}$ and *Irf8*$^{fl/fl}$.*Cd11cCre* mice from the experiment described in (F). All bar graphs in Figure 7 show data as mean ± SEM (*p ≤ 0.05; **p ≤ 0.01; ***p ≤ 0.001), and all data are representative of two independent experiments.

by inducing Toll-like/interleukin-1 receptor signaling. Cardiomyocyte necrosis also results in the release of cardiac self-antigens, such as myosin and troponin, which are constrained in the healthy heart (Larue et al., 1991). Thus, hypothetically, heart DCs become activated via TLR stimulation by danger signals after MI and get loaded with self-antigen, licensing DCs for the activation of self-antigen-specific autoreactive T cells. Indeed, we found that DCs from the infarcted heart and mLN presented cardiac self-antigen to autoreactive $CD4^+$ T cells, which adopted a Th1/Th17 effector phenotype. This suggests that ischemic heart injury leads to cardiac autoimmunity by acting on the DC activation state. Post-infarct autoimmunity is commonly observed, with one-third of patients showing a proliferative response to cardiac myosin (Moraru et al., 2006). Furthermore, post-infarct autoimmunity contributes to persistent myocardial inflammation, leading to further damage with pathological consequences (Gottumukkala et al., 2012). Early after MI (day 2), TCR-M cells proliferated vigorously in heart-draining mLN and, interestingly, also in non-heart draining LNs, which could suggest systemic release of self-antigen post MI due to massive destruction of cardiomyocytes, which is captured by LN-resident DCs. However, we did not observe a significant proliferation of TCR-M cells when co-cultured with bulk spleen or mesenteric LN cells, suggesting that either no systemic αMyHC release occurred or the quantity of self-antigen in the circulation was too low to activate TCR-M cells ex vivo. The proliferated TCR-M cells in distant LNs could possibly also represent recirculating cells that had divided in the heart-draining mLN after their first division.

Among DCs, cDC2s were the main subset activating autoreactive $CD4^+$ T cells post MI and inducing IL-17a and IFNγ in TCR-M cells. Despite this, cDC2s may not be necessary because TCR-M cells also proliferated in the mLN of *Irf4*$^{fl/fl}$*.Cd11cCre* mice, which have a severe reduction in migratory cDC2s. Unfortunately, no perfect model exists, which results in a complete and specific cDC2 ablation because the TFs regulating cDC2 development are still largely unknown and might largely overlap with moDCs and MFs. Although cDC2s highly express IRF4, removal of IRF4 only affects migration of cDC2s (Bajaña et al., 2012). Although we have recently described Zeb2 to be a major TF for cDC2 development, Zeb2 loss only results in ablation of a proportion of cDC2s (Scott et al., 2016).

Overall, we demonstrate that DCs in the ischemic heart are activated and loaded with self-antigen, licensing DCs for efficient autoreactive T cell activation. In the future, it will be of great interest to examine the activation state and function of human DCs isolated from the infarcted heart. This could open the door for therapeutics preventing DC maturation and self-antigen presentation, which could limit the onset of pathological cardiac autoimmunity following MI.

EXPERIMENTAL PROCEDURES

Mice

Wild-type BALB/c mice were purchased from Harlan. αMyHC-TCR transgenic mice (TCR-M) on BALB/c background were provided by B. Ludewig and previously described (Nindl et al., 2012). *Flt3l*$^{-/-}$ mice were on a C57/BL6 background. *Irf4*$^{fl/fl}$*.Cd11cCre* and *Irf8*$^{fl/fl}$*.Cd11cCre* were backcrossed onto the BALB/c background for at least two generations. Mice were used between 5 and 12 weeks of age. The animal ethics committee of Inflammation Research Center (VIB-Ghent University) (IRC) approved all experiments.

Infarct Model

MI was induced by coronary artery ligation in female 8- to 12-week-old mice. Mice were anesthetized with nembutal, moved in the supine position on a heating pad, and intubated. Respiration was started using positive pressure (1.5 L 90 strokes/min), and the left thorax was opened in between the third intercostal space. The pericardium was opened, and the LAD was ligated proximal to the main branching. Discoloration of the ventricle was obvious, indicating proper LAD ligation. Sham operation incorporated all actions, except LAD ligation.

Flow Cytometric Analysis and Sorting

Organs were freshly isolated, and heart ventricles were flushed with PBS. Organs were manually cut in 0.5- to 1-mm pieces using scissors. Samples were enzymatically digested with 20 μg/mL liberase TM (Roche) and 10 U DNase (Roche) in RPMI for 45 min at 37°C. Osmotic lysis buffer was added for 3' to remove erythrocytes. Single-cell suspensions were incubated with a mix of fluorescently labeled monoclonal antibodies (Abs) for 30' at 4°C. To reduce non-specific binding, 2.4G2 Fc receptor Ab was added. An overview of Abs and clones is found in the Supplemental Information. To identify live cells, fixable viability dye eFluor 506 (eBioscience) was added. For intranuclear staining of TFs, cells were fixed using a Foxp3 fixation/permeabilization kit (eBioscience). Data were acquired on an LSR Fortessa cytometer (BD Biosciences). For cell sorting, a FACSAria high-speed sorter (BD Biosciences) was used. Final analysis and graphical output were performed using FlowJo software (Tree Star) and GraphPad Prism.

RNA Sequencing

cDC1s, cDC2s, moDCs, and MFs were sorted by FACS from 100 pooled steady-state and 12 pooled infarcted hearts (7 days post-surgery) of female WT BALB/c mice, and four independent sorts were performed. A maximum of 25,000 cells were sorted directly into 500-μL buffer (RLT Plus; QIAGEN), and 5-μL β-mercaptoethanol and RNA was isolated by using a micro-RNA isolation kit (QIAGEN). Because RNA amounts were low, RNA was amplified using SmarTER amplification (Clontech). RNA sequencing was executed at the Nucleomics facility (VIB) using the NextSeq sequencer (Illumina). RNA-seq was analyzed using Trimmomatic. All details are described in the Supplemental Information.

Adoptive Transfer of TCR-M Cells

Spleens were collected from TCR-M mice and disrupted on a 70-μm cell strainer. Naive TCR-M splenocytes were MACS purified using the $CD4^+CD62L^+$ T Cell isolation kit (Miltenyi). TCR-M cells were labeled with CFSE (Invitrogen). 1×10^6 naive TCR-M T cells were injected intravenously in the lateral tail vein of sham-operated and infarcted mice at day 2 and day 7 after surgery. 3 days after TCR-M adoptive transfer, mice were sacrificed, lymphoid organs were isolated, and cell suspensions were prepared as described for the spleen. CFSE dilution and T cell activation were evaluated by flow cytometry.

Ex Vivo Bulk Lymph Node Co-cultures

Lymph nodes were collected from mice at day 2 or day 7 post surgery. Single-cell suspensions were prepared as described above. 2.5×10^5 bulk LN cells were added to 5×10^4 MACS purified naive $CD4^+CD62L^{hi}$ TCR-M cells that were CFSE labeled. CFSE dilution and T cell activation were evaluated by flow cytometry after 3 days of incubation at 37°C, 5% CO_2, and 20% O_2.

Ex vivo Co-cultures of Sorted DC Subsets and TCR-M Cells

TCR-M cells were purified from the spleen using the $CD4^+$ T Cell isolation kit (Miltenyi) and labeled with CFSE. 5×10^4 TCR-M cells were co-cultured with 1×10^4 FACS-sorted cDC1s, cDC2s, and moDCs from the mediastinal, mesenteric LN, or heart of sham and MI mice (day 7). CFSE dilution and T cell activation were evaluated by flow cytometry after 4 days of incubation at 37°C, 5% CO_2, and 20% O_2. To check Th skewing of TCR-M cells, IL-17A and IFNγ ELISA (eBioscience, Ready-Set-Go kit) was performed on the co-culture cell supernatants.

Statistical Analysis

For all experiments, the difference between groups was calculated using the Mann-Whitney *U* test for unpaired data (GraphPad Prism) and was considered significant when $p < 0.05$.

ACCESSION NUMBERS

The accession number for all RNA-sequencing data reported in this paper is GEO: GSE94949.

SUPPLEMENTAL INFORMATION

Supplemental Information includes Supplemental Experimental Procedures, one figure, and eight tables and can be found with this article online at http://dx.doi.org/10.1016/j.celrep.2017.02.079.

AUTHOR CONTRIBUTIONS

Conceptualization, B.N.L. and P.C.; Methodology, K.V.d.B., D.S., C.L.S., P.C., and M.G.; Formal Analysis; L.M.; Investigation, A.B., J.V.M., M.V., and S.D.P.; Resources, V.N. and B.L.; Writing – Original Draft, K.V.d.B.; Writing – Review & Editing, C.L.S. and B.N.L.; Funding Acquisition, B.N.L. and T.G.; Supervision; B.N.L., T.G., and C.L.S. B.N.L. and P.C. shared supervision over the work.

ACKNOWLEDGMENTS

K.V.d.B. was supported by an AAP fellowship of Ghent University. C.L.S. is supported by a Marie Curie Intra-European Fellowship (IEF; H2020-MSCA-IF-2014 660448). B.N.L. is supported by several FWO grants (Fonds Wetenschappelijk Onderzoek, Vlaanderen) and is the recipient of an ERC consolidator grant (41D04510W).

Received: October 3, 2016
Revised: January 18, 2017
Accepted: February 27, 2017
Published: March 21, 2017

REFERENCES

Anzai, A., Anzai, T., Nagai, S., Maekawa, Y., Naito, K., Kaneko, H., Sugano, Y., Takahashi, T., Abe, H., Mochizuki, S., et al. (2012). Regulatory role of dendritic cells in postinfarction healing and left ventricular remodeling. Circulation *125*, 1234–1245.

Ardouin, L., Luche, H., Chelbi, R., Carpentier, S., Shawket, A., Montanana Sanchis, F., Santa Maria, C., Grenot, P., Alexandre, Y., Grégoire, C., et al. (2016). Broad and largely concordant molecular changes characterize tolerogenic and immunogenic dendritic cell maturation in thymus and periphery. Immunity *45*, 305–318.

Bajaña, S., Roach, K., Turner, S., Paul, J., and Kovats, S. (2012). IRF4 promotes cutaneous dendritic cell migration to lymph nodes during homeostasis and inflammation. J. Immunol. *189*, 3368–3377.

Bajaña, S., Turner, S., Paul, J., Ainsua-Enrich, E., and Kovats, S. (2016). IRF4 and IRF8 act in CD11c+ cells to regulate terminal differentiation of lung tissue dendritic cells. J. Immunol. *196*, 1666–1677.

Caton, M.L., Smith-Raska, M.R., and Reizis, B. (2007). Notch-RBP-J signaling controls the homeostasis of CD8- dendritic cells in the spleen. J. Exp. Med. *204*, 1653–1664.

Darrasse-Jèze, G., Deroubaix, S., Mouquet, H., Victora, G.D., Eisenreich, T., Yao, K.H., Masilamani, R.F., Dustin, M.L., Rudensky, A., Liu, K., and Nussenzweig, M.C. (2009). Feedback control of regulatory T cell homeostasis by dendritic cells in vivo. J. Exp. Med. *206*, 1853–1862.

Davis, M.M. (2015). Not-so-negative selection. Immunity *43*, 833–835.

Epelman, S., Lavine, K.J., Beaudin, A.E., Sojka, D.K., Carrero, J.A., Calderon, B., Brija, T., Gautier, E.L., Ivanov, S., Satpathy, A.T., et al. (2014). Embryonic and adult-derived resident cardiac macrophages are maintained through distinct mechanisms at steady state and during inflammation. Immunity *40*, 91–104.

Eriksson, U., Ricci, R., Hunziker, L., Kurrer, M.O., Oudit, G.Y., Watts, T.H., Sonderegger, I., Bachmaier, K., Kopf, M., and Penninger, J.M. (2003). Dendritic cell-induced autoimmune heart failure requires cooperation between adaptive and innate immunity. Nat. Med. *9*, 1484–1490.

Esterházy, D., Loschko, J., London, M., Jove, V., Oliveira, T.Y., and Mucida, D. (2016). Classical dendritic cells are required for dietary antigen-mediated induction of peripheral T(reg) cells and tolerance. Nat. Immunol. *17*, 545–555.

Gallucci, S., Lolkema, M., and Matzinger, P. (1999). Natural adjuvants: endogenous activators of dendritic cells. Nat. Med. *5*, 1249–1255.

Gangaplara, A., Massilamany, C., Brown, D.M., Delhon, G., Pattnaik, A.K., Chapman, N., Rose, N., Steffen, D., and Reddy, J. (2012). Coxsackievirus B3 infection leads to the generation of cardiac myosin heavy chain-α-reactive CD4 T cells in A/J mice. Clin. Immunol. *144*, 237–249.

Ganguly, D., Haak, S., Sisirak, V., and Reizis, B. (2013). The role of dendritic cells in autoimmunity. Nat. Rev. Immunol. *13*, 566–577.

Gawden-Bone, C., Zhou, Z., King, E., Prescott, A., Watts, C., and Lucocq, J. (2010). Dendritic cell podosomes are protrusive and invade the extracellular matrix using metalloproteinase MMP-14. J. Cell Sci. *123*, 1427–1437.

Gottumukkala, R.V., Lv, H., Cornivelli, L., Wagers, A.J., Kwong, R.Y., Bronson, R., Stewart, G.C., Schulze, P.C., Chutkow, W., Wolpert, H.A., et al. (2012). Myocardial infarction triggers chronic cardiac autoimmunity in type 1 diabetes. Sci. Transl. Med. *4*, 138ra80.

Guilliams, M., Ginhoux, F., Jakubzick, C., Naik, S.H., Onai, N., Schraml, B.U., Segura, E., Tussiwand, R., and Yona, S. (2014). Dendritic cells, monocytes and macrophages: a unified nomenclature based on ontogeny. Nat. Rev. Immunol. *14*, 571–578.

Guilliams, M., Dutertre, C.A., Scott, C.L., McGovern, N., Sichien, D., Chakarov, S., Van Gassen, S., Chen, J., Poidinger, M., De Prijck, S., et al. (2016). Unsupervised high-dimensional analysis aligns dendritic cells across tissues and species. Immunity *45*, 669–684.

Gurka, S., Hartung, E., Becker, M., and Kroczek, R.A. (2015). Mouse conventional dendritic cells can be universally classified based on the mutually exclusive expression of XCR1 and SIRPα. Front. Immunol. *6*, 35.

Hart, D.N., and Fabre, J.W. (1981). Demonstration and characterization of Ia-positive dendritic cells in the interstitial connective tissues of rat heart and other tissues, but not brain. J. Exp. Med. *154*, 347–361.

Heinz, L.X., Baumann, C.L., Köberlin, M.S., Snijder, B., Gawish, R., Shui, G., Sharif, O., Aspalter, I.M., Müller, A.C., Kandasamy, R.K., et al. (2015). The lipid-modifying enzyme SMPDL3B negatively regulates innate immunity. Cell Rep. *11*, 1919–1928.

Holst, K., Guseva, D., Schindler, S., Sixt, M., Braun, A., Chopra, H., Pabst, O., and Ponimaskin, E. (2015). The serotonin receptor 5-HT_7R regulates the morphology and migratory properties of dendritic cells. J. Cell Sci. *128*, 2866–2880.

Kool, M., van Loo, G., Waelput, W., De Prijck, S., Muskens, F., Sze, M., van Praet, J., Branco-Madeira, F., Janssens, S., Reizis, B., et al. (2011). The ubiquitin-editing protein A20 prevents dendritic cell activation, recognition of apoptotic cells, and systemic autoimmunity. Immunity *35*, 82–96.

Larue, C., Calzolari, C., Léger, J., Léger, J., and Pau, B. (1991). Immunoradiometric assay of myosin heavy chain fragments in plasma for investigation of myocardial infarction. Clin. Chem. *37*, 78–82.

Latet, S.C., Hoymans, V.Y., Van Herck, P.L., and Vrints, C.J. (2015). The cellular immune system in the post-myocardial infarction repair process. Int. J. Cardiol. *179*, 240–247.

Lipes, M.A., and Galderisi, A. (2015). Cardiac autoimmunity as a novel biomarker, mediator, and therapeutic target of heart disease in type 1 diabetes. Curr. Diab. Rep. *15*, 30.

Lv, H., and Lipes, M.A. (2012). Role of impaired central tolerance to α-myosin in inflammatory heart disease. Trends Cardiovasc. Med. *22*, 113–117.

Lv, H., Havari, E., Pinto, S., Gottumukkala, R.V., Cornivelli, L., Raddassi, K., Matsui, T., Rosenzweig, A., Bronson, R.T., Smith, R., et al. (2011). Impaired

thymic tolerance to α-myosin directs autoimmunity to the heart in mice and humans. J. Clin. Invest. *121*, 1561–1573.

Maekawa, Y., Mizue, N., Chan, A., Shi, Y., Liu, Y., Dawood, S., Chen, M., Dawood, F., de Couto, G., Li, G.H., et al. (2009). Survival and cardiac remodeling after myocardial infarction are critically dependent on the host innate immune interleukin-1 receptor-associated kinase-4 signaling: a regulator of bone marrow-derived dendritic cells. Circulation *120*, 1401–1414.

Magister, S., Obermajer, N., Mirković, B., Svajger, U., Renko, M., Softić, A., Romih, R., Colbert, J.D., Watts, C., and Kos, J. (2012). Regulation of cathepsins S and L by cystatin F during maturation of dendritic cells. Eur. J. Cell Biol. *91*, 391–401.

Mildner, A., and Jung, S. (2014). Development and function of dendritic cell subsets. Immunity *40*, 642–656.

Miller, J.C., Brown, B.D., Shay, T., Gautier, E.L., Jojic, V., Cohain, A., Pandey, G., Leboeuf, M., Elpek, K.G., Helft, J., et al.; Immunological Genome Consortium (2012). Deciphering the transcriptional network of the dendritic cell lineage. Nat. Immunol. *13*, 888–899.

Molawi, K., Wolf, Y., Kandalla, P.K., Favret, J., Hagemeyer, N., Frenzel, K., Pinto, A.R., Klapproth, K., Henri, S., Malissen, B., et al. (2014). Progressive replacement of embryo-derived cardiac macrophages with age. J. Exp. Med. *211*, 2151–2158.

Moraru, M., Roth, A., Keren, G., and George, J. (2006). Cellular autoimmunity to cardiac myosin in patients with a recent myocardial infarction. Int. J. Cardiol. *107*, 61–66.

Nindl, V., Maier, R., Ratering, D., De Giuli, R., Züst, R., Thiel, V., Scandella, E., Di Padova, F., Kopf, M., Rudin, M., et al. (2012). Cooperation of Th1 and Th17 cells determines transition from autoimmune myocarditis to dilated cardiomyopathy. Eur. J. Immunol. *42*, 2311–2321.

Ohl, L., Mohaupt, M., Czeloth, N., Hintzen, G., Kiafard, Z., Zwirner, J., Blankenstein, T., Henning, G., and Förster, R. (2004). CCR7 governs skin dendritic cell migration under inflammatory and steady-state conditions. Immunity *21*, 279–288.

Ohnmacht, C., Pullner, A., King, S.B.S., Drexler, I., Meier, S., Brocker, T., and Voehringer, D. (2009). Constitutive ablation of dendritic cells breaks self-tolerance of CD4 T cells and results in spontaneous fatal autoimmunity. J. Exp. Med. *206*, 549–559.

Persson, E.K., Uronen-Hansson, H., Semmrich, M., Rivollier, A., Hägerbrand, K., Marsal, J., Gudjonsson, S., Håkansson, U., Reizis, B., Kotarsky, K., et al. (2013). IRF4 transcription-factor-dependent CD103(+)CD11b(+) dendritic cells drive mucosal T helper 17 cell differentiation. Immunity *38*, 958–969.

Scaffidi, P., Misteli, T., and Bianchi, M.E. (2002). Release of chromatin protein HMGB1 by necrotic cells triggers inflammation. Nature *418*, 191–195.

Scott, C.L., Bain, C.C., Wright, P.B., Sichien, D., Kotarsky, K., Persson, E.K., Luda, K., Guilliams, M., Lambrecht, B.N., Agace, W.W., et al. (2015). CCR2(+)CD103(-) intestinal dendritic cells develop from DC-committed precursors and induce interleukin-17 production by T cells. Mucosal Immunol. *8*, 327–339.

Scott, C.L., Soen, B., Martens, L., Skrypek, N., Saelens, W., Taminau, J., Blancke, G., Van Isterdael, G., Huylebroeck, D., Haigh, J., et al. (2016). The transcription factor Zeb2 regulates development of conventional and plasmacytoid DCs by repressing Id2. J. Exp. Med. *213*, 897–911.

Sichien, D., Scott, C.L., Martens, L., Vanderkerken, M., Van Gassen, S., Plantinga, M., Joeris, T., De Prijck, S., Vanhoutte, L., Vanheerswynghels, M., et al. (2016). IRF8 transcription factor controls survival and function of terminally differentiated conventional and plasmacytoid dendritic cells, respectively. Immunity *45*, 626–640.

Sichien, D., Lambrecht, B.N., Guilliams, M., and Scott, C.L. (2017). Development of conventional dendritic cells: from common bone marrow progenitors to multiple subsets in peripheral tissues. Mucosal Immunol. Published online February 15, 2017. http://dx.doi.org/10.1038/mi.2017.8.

Steinman, R.M., Hawiger, D., and Nussenzweig, M.C. (2003). Tolerogenic dendritic cells. Annu. Rev. Immunol. *21*, 685–711.

Stranges, P.B., Watson, J., Cooper, C.J., Choisy-Rossi, C.M., Stonebraker, A.C., Beighton, R.A., Hartig, H., Sundberg, J.P., Servick, S., Kaufmann, G., et al. (2007). Elimination of antigen-presenting cells and autoreactive T cells by Fas contributes to prevention of autoimmunity. Immunity *26*, 629–641.

Tamoutounour, S., Guilliams, M., Montanana Sanchis, F., Liu, H., Terhorst, D., Malosse, C., Pollet, E., Ardouin, L., Luche, H., Sanchez, C., et al. (2013). Origins and functional specialization of macrophages and of conventional and monocyte-derived dendritic cells in mouse skin. Immunity *39*, 925–938.

Tian, W., Nunez, R., Cheng, S., Ding, Y., Tumang, J., Lyddane, C., Roman, C., and Liou, H.C. (2005). C-type lectin OCILRP2/Clr-g and its ligand NKRP1f costimulate T cell proliferation and IL-2 production. Cell. Immunol. *234*, 39–53.

Torchinsky, M.B., Garaude, J., Martin, A.P., and Blander, J.M. (2009). Innate immune recognition of infected apoptotic cells directs T(H)17 cell differentiation. Nature *458*, 78–82.

Waskow, C., Liu, K., Darrasse-Jèze, G., Guermonprez, P., Ginhoux, F., Merad, M., Shengelia, T., Yao, K., and Nussenzweig, M. (2008). The receptor tyrosine kinase Flt3 is required for dendritic cell development in peripheral lymphoid tissues. Nat. Immunol. *9*, 676–683.

Wu, X., Briseño, C.G., Durai, V., Albring, J.C., Haldar, M., Bagadia, P., Kim, K.W., Randolph, G.J., Murphy, T.L., and Murphy, K.M. (2016). Mafb lineage tracing to distinguish macrophages from other immune lineages reveals dual identity of Langerhans cells. J. Exp. Med. *213*, 2553–2565.

Zhang, J., Yu, Z.X., Fujita, S., Yamaguchi, M.L., and Ferrans, V.J. (1993). Interstitial dendritic cells of the rat heart. Quantitative and ultrastructural changes in experimental myocardial infarction. Circulation *87*, 909–920.

Zhang, W., Lavine, K.J., Epelman, S., Evans, S.A., Weinheimer, C.J., Barger, P.M., and Mann, D.L. (2015). Necrotic myocardial cells release damage-associated molecular patterns that provoke fibroblast activation in vitro and trigger myocardial inflammation and fibrosis in vivo. J. Am. Heart Assoc. *4*, e001993.

Zigmond, E., Samia-Grinberg, S., Pasmanik-Chor, M., Brazowski, E., Shibolet, O., Halpern, Z., and Varol, C. (2014). Infiltrating monocyte-derived macrophages and resident kupffer cells display different ontogeny and functions in acute liver injury. J. Immunol. *193*, 344–353.

Cell Reports, Volume *18*

Supplemental Information

Myocardial Infarction Primes Autoreactive T Cells through Activation of Dendritic Cells

Katrien Van der Borght, Charlotte L. Scott, Veronika Nindl, Ann Bouché, Liesbet Martens, Dorine Sichien, Justine Van Moorleghem, Manon Vanheerswynghels, Sofie De Prijck, Yvan Saeys, Burkhard Ludewig, Thierry Gillebert, Martin Guilliams, Peter Carmeliet, and Bart N. Lambrecht

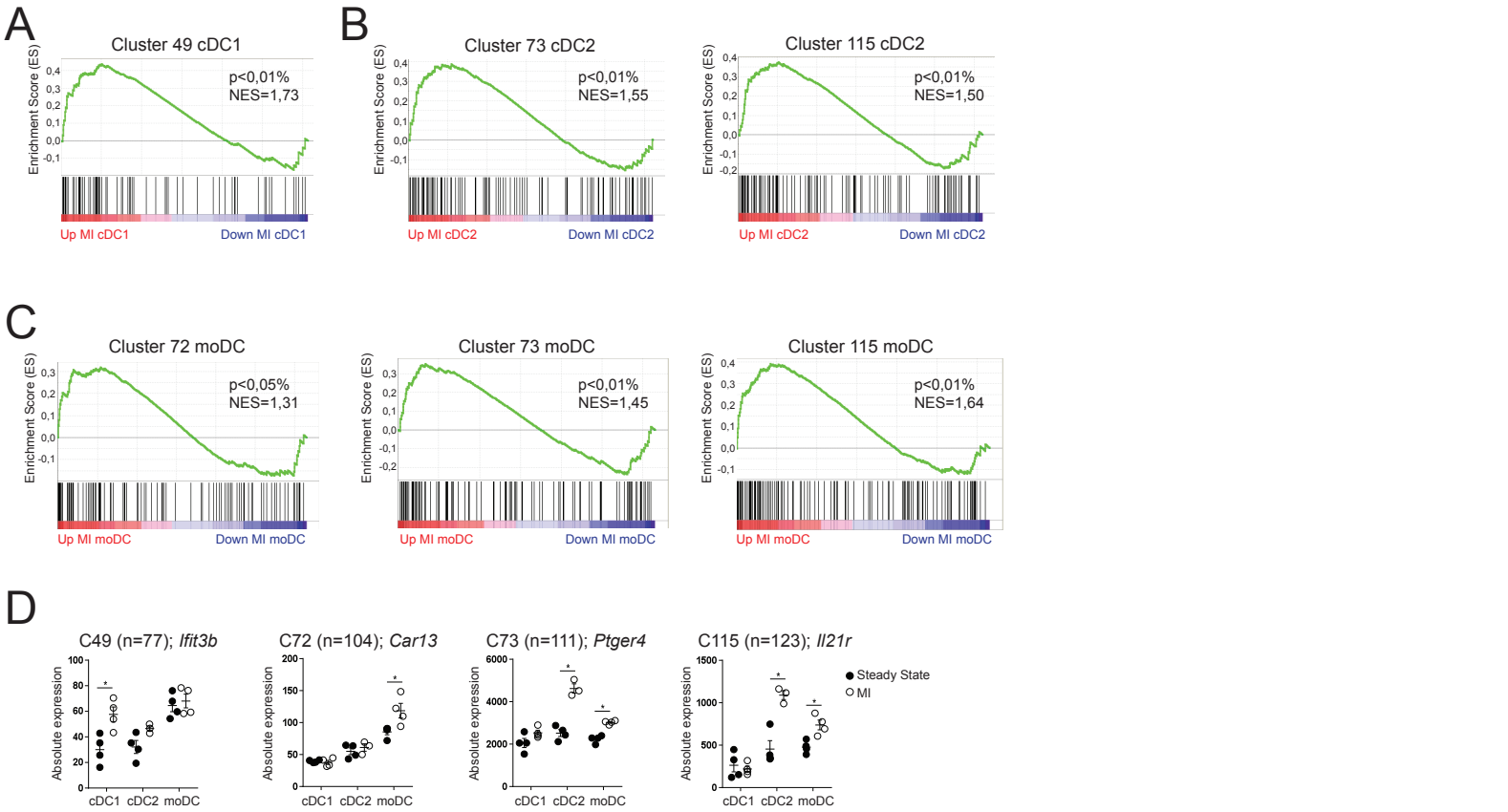

Figure S1. Related to Figure 5.

Gene Set Enrichment Analysis (GSEA) shows the similarity that is found in the upregulation of genes in specific DC subsets from steady state heart to DC subsets from infarcted heart at day 7 post MI with gene clusters that are upregulated in TLR-induced and homeostatic maturation (Ardouin et al, 2016). The resulting enrichment plots are shown in (A-C), as well as the corresponding values of normalized enrichment scores (NES) and false discovery rates (p). (A) Cluster 49 represents genes that are upregulated specifically in TLR-induced maturation. Highly significant enrichment of C49 genes is observed in cDC1s from MI d7 heart. (B) Cluster 73 and 115 represent genes upregulated both in TLR-induced and homeostatic maturation and were found to be significantly enriched in cDC2s from MI d7 heart compared to cDC2s from steady state heart. (C) Clusters 72, 73 and C115 are significantly enriched in heart moDCs at day 7 post MIcompared to heart moDCs in steady state. C72 is also enriched in TLR-induced and homeostatic maturation. (D) Absolute expression of respresentative genes fromC49, C72, C73 and C115 which are enriched in specific DC subsets at day 7 post MI compared to steady state (Mean±SEM; $p<0.05$).

Table S1a. Related to Figure 5 **Differentially expressed genes: St St vs MI cDC1s**

Up-regulated		Down-regulated	
Flot1	Cacna1s	Cxx1a	Clec5a
Emb	Tcta	Tlr2	Cytl1
Wfdc17	Ednra	Fam65b	Aspn
Lpar1	Tmem159	Gadd45g	Icosl
Plac8	Ano1	Pde2a	Rasl11b
Ifitm1	Rapgef3	Rbp7	Rasl12
Tdgf1	Parva	Hsp90aa1	Gata2
Ifitm2	Hbegf	Cfh	S100a10
Casp6	Bcl6b	Slc25a29	Pstpip2
Pla2g7	Bbc3	Adcy6	Stmn2
Dok3	Lyz2	Pkia	Adgrg1
Ank1	Mob3c	Gucy1b3	Arpin
0610040J01Rik	Cyp8b1	Slc28a2	Pde1b
Prss57	Stambpl1	Ebi3	Cav2
Tmem173	Slc16a2	Ctsw	Zfp862-ps
Dpy19l3	Zfp867	Crim1	Cyp2s1
Fcrlb	Dusp2	Lum	Itga7
Arhgef10	Hvcn1	Yap1	St6galnac3
Ptgdr2	Vcam1	Serpina3f	Tspan7
Jak3	Dnaja1	Otof	S1pr3
P2ry1	Kdr	Ifnlr1	Arhgap29
Lefty1	Cd101	Mpzl2	Abca9
Dip2c	Nrarp	Hs3st1	Afap1l1
Zdhhc23	Dedd2	Pdlim3	Sertad1
Itga6	Sncg	Fndc4	Trim2
Chac1	Treml4	Zbtb32	4930502E18Rik
Smad7	Dll4	Trib2	Cd163
F830002L21Rik	Ldb2	Atf4	Ctnnd1
Plet1	Trf	Pik3r3	Tnfrsf9
Camkk1	Bend6	Lox	Abcc9
Xxylt1	Ncr1	Gimap1	Irf1
Slc8a1	Nfkbie	Hspa1l	Ptprm
Gpr4	Egr1	Ncf2	Phldb2
Htr7	Cygb	Gper1	Il1a
Plscr1	Epcam	Egfl7	Pxdn
Btbd11	Efnb2	Pygm	Mmp15
Ier3	Gm11837	Slc2a4	Tns1
Ctnnd2	Serping1	Ppap2b	Gbp2
Lgmn	S100a16	Etv1	Slc5a3
Gpr171	Hmox1	Spata13	St5
Palm	Susd5	Slc26a10	Aldh1a2
Ptpn1	Ldhb	Hspa1a	St6gal1
Ggt5	Ccl9	Zfp296	Tnfsf9
Nxpe3	Fam101b	Fzd4	Cdc42ep1
Scamp1	Gphn	Mcam	Hspa1b
Ccl7	Ndufa4l2	Map3k7cl	Sorbs1
Mmp14	Ctgf	Tnni3	Flrt3
Gpsm2	Gcnt2	Il1rl1	Tnfsf8
Syt11	Serpinb6b	Hey1	Myl9
Pik3cd	Wnt11	Gprc5a	Tns2
Bcl11a	Jun	Sult1a1	Entpd1
BC021614	Tacc2	Mb	Txnip
Ubr4	Fas	Ccnd2	Clec4a2
	Myl3	Cd81	Cd300lg

Table S1b. Related to Figure 5 **Differentially expressed genes: St St vs MI cDC1s**

Down-regulated			
Spn	Aqp7	Aoc3	Ccdc3
Zc3h12a	Clec4b1	Axl	Pdlim1
Adgre1	Mgp	Sema3g	Olfr558
Dcstamp	Sox17	Lims2	Nkg7
Wwtr1	Steap4	Dnajb4	Gas6
Sspn	Kcnab1	Ltb4r1	Tpm2
Atp8b1	Jam3	Timp2	Ptprb
Frmd4b	Msrb3	Cav1	Serpinb10
Igfbp5	Arhgef3	Esam	Dok2
Serpinb8	Gimap4	Aqp1	Cldn5
Fhl1	Il12rb2	Cyr61	Il2rb
Gem	Ddit4	Ltbp4	Tinagl1
Ly6a	Fndc7	Trim47	Sparc
Eng	Mmrn2	Mfge8	Ptrf
Mcemp1	Gypc	Nfkbiz	Rgs4
Egflam	Mgll	9430020K01Rik	Gja5
Nfkbia	Alpl	Rhoj	Ets1
Rin2	Phlda1	Tmem47	Tagln
Clu	Emp2	Mmp19	
Hsph1	Xlr	Nrip2	
Cers4	Crip2	S1pr1	
Plau	Lmna	Cd1d1	
Cd34	Nfkbid	Tnf	
Dnase1l3	Plxdc2	Dnajb1	
Pltp	Sulf1	Mamdc2	
Dysf	Sema6d	Tnfsf13b	
L1cam	Ptpro	Ablim1	
Cd8a	Adgrf5	Pcp4l1	
Gadd45b	Bag3	Naalad2	
Tcf15	Tnfaip2	Lamb2	
Tbx2	Apold1	Cd209a	
Col3a1	Rasl11a	Clec14a	
Ccl17	Tmem204	Aplnr	
Tesc	Nppa	Igfbp4	
Eln	Sod3	Epas1	
Emp1	Pdgfrb	Jam2	
Fam198b	Kitl	Ly6c1	
Sdcbp2	Col4a1	Lpl	
Ephx1	Ace	Gzma	
Cald1	Sox18	Nedd4	
Gfra2	Timd4	Id3	
Smpdl3b	Gstm1	Prf1	
Grap	Fstl1	She	
Arhgef15	Gm13889	Htra1	
Tppp3	Tie1	Pecam1	
Gpihbp1	F11r	Ephb4	
Rhof	Cdh13	Cd93	
Col8a1	Fermt2	Mustn1	
Cnn1	Hes1	Gucy1a3	
Hspa12b	Bcam	Ly6e	
Lamc1	Gimap6	Adam23	
Slc11a1	Zfand2a	Pcdh7	
Sh3pxd2a	Cd207	Serpinh1	
Sell	Sdc1	Nppc	

Table S2a. Related to Figure 5 **Differentially expressed genes: St St vs MI cDC2s**

Up-regulated				
Fxyd7	1110032F04Rik	Spsb1	Klrc1	Nedd4l
Ifitm1	Fads2	Siglece	Zmynd15	Mif4gd
Slc16a14	St8sia1	Dab2	Mfsd6	Bmf
Enpp1	Gcnt1	2510009E07Rik	Amacr	Gpr137b
Ffar2	Lsr	Myo1b	Wwc2	Sestd1
Cdh1	Soat2	Lpar3	Cux1	Clec5a
Rptoros	Kit	Il21r	Ubr4	Cdc14a
Card11	Ly75	Hrh2	Sh3pxd2b	Bmp2k
Zbtb18	Gpr162	Adam23	Gpr4	Cog7
Lgi4	Actn1	Prss30	Dennd3	Gnptab
2900026A02Rik	Gprc5c	Ffar4	Pdk1	Atp6v0a1
Cep170b	Ifit1	Igfbp6	Osbpl7	Lmtk2
Ppm1j	Gm7609	Flt3	Cd33	Ltb
Dscam	Cd300lf	Jak3	Fmnl3	Gstt3
Ctnnd2	A530032D15Rik	0610040J01Rik	Bst1	Cpd
Tmem231	Tnfrsf4	Rnf157	Gpr171	Soga1
Ocln	Ccr6	Tmem158	Grasp	Rogdi
Cyp7b1	Htra3	Plxnc1	Ifit2	Tgfbi
Entpd3	Galnt12	Gdf15	Cdyl2	Hdac6
Timp1	Numa1	Sulf2	Dhfr	Ptprs
Galnt6	Msantd1	Btla	Cpne2	Asxl1
Lox	Fads3	Hpgds	Acvr2a	Abhd15
Il1r2	Ccnjl	Mov10	Slc12a7	Gpr183
Angptl2	Upp1	Casp6	6330416G13Rik	Ciita
Mreg	Hip1r	Spint2	Mink1	Arhgap22
Plekha5	Tbc1d16	Pxdc1	Arid2	Ssh1
Dbn1	Nav2	Dock4	Agap1	Anpep
Spon1	Shisa9	Atp8b1	Ttyh2	Slfn5
Htr7	Cttnbp2nl	Selp	Cxcl16	Fam3c
Cd72	Timd4	2010315B03Rik	St8sia6	Knop1
Mmp14	Basp1	Itga6	Bach2	1700021K19Rik
Il2ra	Slc22a23	Klrb1c	Ccdc88b	Rrad
Gpnmb	Il7r	Hivep2	Slc14a1	Syt11
Trp53i11	Ssx2ip	Spns3	Nbeal2	Csf2rb2
Tnfsf4	Klrb1b	Pik3cb	Fam134b	Tmem173
Dmkn	Zfp366	Kif1a	Ipcef1	Smad7
Tmem150c	Cd38	Slc7a11	Hexb	Tns3
Epcam	Aatk	Stk38l	Clec4n	Creb5
A4galt	Stil	Ppp1r3b	Med13l	Arap3
Spp1	Scin	Ddr1	Ptgs2	
Pram1	Pdlim7	Fbrsl1	Map4k3	
Arhgef40	Tbc1d4	Nxpe5	Gab2	
Gpr82	Fnip2	Stat4	Capn15	
Syngr1	Rtn4rl1	Pvrl4	Trp53bp1	
Scel	Apbb2	Itpr3	Ifit3	
F11r	Uvssa	Zdhhc23	Ptger4	
Ggt5	Flot1	Calcrl	Myh9	
Prune2	Cst7	Klrd1	8430419L09Rik	
Il18rap	Klrb1f	Lin9	Uck2	
Rgs12	H2-Oa	Smarca2	B3gnt8	
Adam11	Myo1e	Gga2	Foxj2	
Abcb4	Ttll5	Atp8a1	Jak2	
Dkkl1	Cul7	Klra3	Dock5	
Arhgap24	Tjp3	Zeb1	Fcgr1	
Plscr1	Cxxc5	Galm	Vsig10	

Table S2b. Related to Figure 5 **Differentially expressed genes: St St vs MI cDC2s**

Down-regulated

Ahcyl2	Vps9d1	Tbxas1	Serpinb8	Xlr	Sparc	Cers4
Igfbp4	Crim1	Ptgir	Rhob	Adamts1	Negr1	Cp
Il18	Ldlr	Hr	Smpdl3b	Fcrl1	Epha10	Ptrf
Bcl2a1a	Synpo	Nsl1	Mrps6	Tmem71	BC035044	Ryk
Slc22a5	Mad2l1bp	Lonrf1	Gcc1	Tlr11	Gfra2	Igfbp7
Aif1	Id1	Rffl	Rnd1	Slc4a5	Sectm1a	Tppp
Eif5	F10	Cxx1c	Pla2g16	Acta2	Kank3	Tinagl1
Cxcl1	Mir22hg	Ifitm6	Slc13a3	Ldlrad1	Cracr2b	Nxpe4
Oxct1	Adam8	Tsc22d3	Sgms2	Cdc42ep1	Cd209d	Abcg3
Acot9	Cks2	Bbc3	Tnfaip6	Col14a1	Slc9a4	Adamdec1
Ttc39b	Rras	Rab20	Cxcl10	Dnaja1	Sdc1	Tppp3
Tmem159	Plxdc1	St3gal3	Itga9	Akr1c13	4930455G09Rik	Lpl
Cd84	Tns1	Phlda3	Nrg2	Olfr1033	Thsd4	Efnb2
Rxra	Pwwp2b	Tsc22d1	Rgcc	Crip2	Colec12	E230016K23Rik
Tmem62	Rab7b	Rbpms	Msrb3	Sec16b	Tmem229a	Rem1
Plau	Mpeg1	Gbp3	Sqrdl	Cd300lb	Rasl11b	Bag3
St3gal1	Hic2	Plaur	Bcam	Plxna4	Fabp7	Pf4
Dgat2	Hspe1	Tarsl2	Icam1	Tmcc1	Etv1	Ehd2
Prr5l	Pira6	Adgre1	Hspa1a	Ncr1	Nkg7	Omp
Rhot2	Tnfsf14	Nr1h3	Ccl9	Pilra	Il27ra	Spic
Mtmr10	Pde2a	Gpr84	Nos3	Mgst1	Cd79a	Hes1
Dram1	Serpinb6a	Dnajb4	Lmna	Trf	Ets1	Prf1
Clec4e	Zfand2a	Nod1	Phlda1	Mxra7	Kitl	Ak8
Cd300ld	Fcgr3	Nedd4	Adrb1	Espn	Cebpe	Lyz2
Ltb4r1	Arhgef10l	Clec4g	Hnmt	Rgs4	Plcb1	A530064D06Rik
Zswim6	Adssl1	Batf	Ldlrad3	Dpy19l3	Celf4	Hepacam2
Socs6	Glrx	Fn1	Gimap4	Gypc	Myl3	Kazald1
Itgb3	Pla2g7	Id3	Prdm16	Stox2	Tspan7	Dmpk
Txnip	Stard4	Sgms1	Col4a1	Cd300e	Tmem26	Nfe2
Sertad1	Hsp90aa1	Maf	Adgre5	Tm4sf1	Dok2	Spink2
Daglb	Areg	Ifrd1	Fgd4	Tnfaip8l1	Hey1	Serpinb10
Slc16a1	Slc5a3	St3gal6	Sh3bp5	Sphk1	Sv2b	Slc12a2
Tnfaip2	Dusp10	Tmeff1	Grap	Gas7	Aplnr	F3
Ppt2	Capn5	Mturn	Trem3	Vcam1	Rorc	Ptger2
Unc119	Rnasel	Thbd	Crem	Abcd2	Hcar2	Hopx
Tubb6	Cd300lg	Lmo1	Dleu2	Cd163	Atp1a3	Gjb2
Tspan33	C5ar1	Tmem154	Dusp6	Pilrb1	Slc11a1	Slc15a2
Cd44	Apoe	Selenbp1	Ccl2	Ryr1	Gprc5a	Ccdc149
Mt1	Dedd2	Ccr9	Cma1	Cxcl9	Il1a	Treml4
Adrb2	Bank1	Olfml3	Nupr1	Ceacam1	Klrb1a	Rnase2a
Crat	St3gal5	Tnfsf13b	Grk5	Gfi1b	Fabp4	Cd81
Mapk6	Cyp4f18	March8	Zfyve9	Acy1	Sh2d2a	Lrrc3
Ccdc117	Pparg	Icam2	Hbegf	Oasl1	Ly6e	Ly6c2
Slfn2	Ifi27l2a	Kcne3	Mefv	Has1	Pde12	Cdc42ep2
Rbm48	Crip1	Sept11	Gbp8	Gm21188	Il1rn	Klra2
Gpsm2	Tpst2	Fam20a	Hsph1	Pkdcc	Hspa1b	Pglyrp1
Ctsf	Gbp9	Klhl13	Ikzf3	Fpr2	Fzd4	Ccdc170
Notch1	Atf4	Sult1a1	Clec9a	Gpihbp1	Ica1l	Ear2
Cib1	Capg	Trim41	Fcrls	Fgd6	Cish	Cd209b
Klf2	Mmp19	Clec4f	Cd36	Pilrb2	Ccl6	Ephx1
Cpq	S1pr4	Gas6	Lyz1	Chrna5	Gm14085	Arhgef37
Batf3	Plxdc2	Rarb	Kcnq1	Gm6297	Ankrd13b	Ace
Rilpl2	Cd177	Gpr65	Cd2	Mras	Ndnf	Hmox1
Gbp2	Tlr7	Ccr3	Akr1c18	Cnn3	Wnt11	Otof
Sat1	Folr2	Alox15	Hspb1	Steap3	Slco2b1	Sema4b
Tfdp2	Hes2	Itk	Hpgd	Cyr61	Serpinb2	F13a1
Sepp1	Gbp4	Cebpb	Retnla	Upb1	Slc27a3	C4b
Camkk2	Ccl7	1810011O10Rik	Gzma	Cd226	Nrarp	
Rasgrp2	Slc28a2	Ccl24	Pdlim1	Mmp13	Timp3	
Trpm2	Sgce	Il2rb	Lgi3	Il6	Mamdc2	
Steap4	Ecm1	Hsd11b1	P3h2	Itgal	Dnajb1	
Crym	Adgre4	Hebp2	Jchain	Aldh1a2	Galnt9	
Mt2	Tlr12	Ptgs1	Rnf144a	Thbs1	Ms4a8a	
Agpat3	Lilra5	9830107B12Rik	Cyp2ab1	Lck	Cd207	

Table S3. Related to Figure 5 **Differentially expressed genes: St St vs MI moDCs**

Up-regulated			Down-regulated		
Fxyd7	Ndnf	Cd226	Slc22a18	Mgll	Pla2g2d
Fam83f	Adgre5	Lpin1	Syt3	Gas6	Mtmr11
Zbtb18	Ly6e	Hs3st3a1	Cd209d	Dpysl3	Agpat3
Ifnlr1	Gas1	Trp53rka	Ephx3	Cav1	Tnni3
Stat4	Smarcd3	Fbp1	Ptk2	Tmem26	Adamdec1
Nt5e	Thrsp	Tln2	Fxyd2	Cables1	Ckm
Spon1	Igf1	Slc2a4	Serpine1	Tlr12	Mxra8
Tnfrsf9	Sh3bp5	Csf1	Wtip	Vcam1	Alpl
Arhgap24	Cish	Adcy4	Il6	Smpdl3b	St3gal6
Il7r	Mycl	Ear2	Cxx1c	Folr2	Slco2b1
Prss46	Cdc42ep2	Cdkn1c	Crip2	Nkg7	Igfbp4
Htr7	Fam101b	Ablim1	Tmem204	Tmem47	Tgfbr3
Galnt6	Dusp7	Mmp2	Bcl6b	Iigp1	Nrip2
Tmem158	Fam43a	Asb10	Gm13889	Dnajb4	Dnaja1
Cxcr3	Lyz1	Sema4c	Cxcr2	Prf1	Cxcl12
Lgi4	Hdc	9430015G10Rik	Hbegf	Lck	Lims2
Plxnc1	Tnnt2	Unc5b	Tek	Id3	Stard13
Cdk18	Myl9	Itga9	Hspg2	Hey1	Gpr165
2900026A02Rik	Ptp4a3	Cuedc1	Rasl12	Atp9a	Grap
Angptl2	Dedd2	Timp3	S100a16	Cd2	Slc12a2
Gpc1	St3gal1	Mrvi1	P2ry13	Gm14085	Cdc42ep1
Rai14	Ebi3	Msrb3	Tagln	Rgl3	Hsph1
Mmp14	Gbp9	Smagp	Fam65b	Mustn1	Slc27a6
Ndrg1	Tbx20	Gprc5a	Ndrg2	Gm6297	Etv1
Plscr1	Tmcc1	Cxcr6	Cyr61	Fabp3	Myl2
Ifit2	Maf	Ptprg	P3h2	Adgrl2	Clic5
Slc7a11	Ddah2	Ltbp4	Cracr2b	Slc28a2	Apold1
Fbxl2	Unc13b	Epas1	Neurl1a	Clec4f	Actc1
Fam132a	Npnt	Spic	Trpv4	Nedd4	Pf4
Map4k3	Lhfp	Mag	Ctsf	Pyroxd2	
Slc27a1	Asb2	Crim1	Gm4951	Serpinh1	
Anpep	Alox15	Ly6a	Cyp2ab1	Adgrl4	
Ms4a7	AW011738	Rhobtb1	Fzd4	Cbr2	
Nxpe5	Txnip	Tmod1	She	Perp	
Dock5	Oasl1	Trpm2	Fcrls	Tpm2	
Cdh1	Tppp3	Serpinb8	Sept4	Mylk	
Aatk	Heg1	Icam2	Gpihbp1	Klra2	
Il18rap	Tsc22d3	Rnf144a	Fbln2	Afap1l1	
Ramp3	Igf2bp3	Nid2	Capn3	Cdh5	
Scin	Gcc1	Tmem45b	Chp2	F13a1	
Gcnt1	Adrb2	Ly6c2	Id1	BC035044	
	Rgs5	Ly6c1	Bcam	Cd207	
	8430408G22Rik	Mb	Lilra5	Crym	
	Adgre4	Aqp7	Hpgd	Adamts1	
	Gbp4	Hspa1a	Slc15a2	Myoz2	
	Mmp9	Sult1a1	Agmo	Ephx1	
	Tppp	Gja4	Cd36	Ptrf	
	Acta2	Xlr	Hcar2	Pln	
	Cxcl13	Igf2	Ets1	Alox5	
	Itgal	Kcnq1	Cd81	Cd34	
	Fabp4	Sdpr	Mmp13	Cdr2	
	C1qtnf1	Bag3	Tnfsf13b	Myl7	
	Mxra7	Itga7	Nppa	Rhoj	
	Epor	Ehd2	Ppp1r9a	Cald1	
	Serpinf1	Cd209b	Pdlim1	Adgrg1	
	Sparcl1	Ildr2	Adrb1	Cmah	
	Gzma	Hepacam2	Il1a	Cp	
	Klhl13	Cd163	Celf4	Hspb1	
	Lrrc3	Mucl1	Ptgs1	Dmpk	
	Nrarp	Heyl	Egfl7	Sorbs2	
	Bank1	Vsig4	Nos3	Slc9a3r2	
	Retnla	1810011O10Rik	Gm4980	Gja5	
	Tspan7	Hes1	Myl3	Dnajb1	
	Sgce	Hspa1b	Hs3st1	Il2rb	

Table S4. Related to Figure 5 **54 differentially expressed genes: St St vs MI cDC1s, cDC2s and moDCs**

Up-regulated		Down-regulated		
Htr7	Ly6e	Gas6	Cdc42ep1	Bag3
Mmp14	Dedd2	Vcam1	Hsph1	Hspa1a
Plscr1	Txnip	Smpdl3b	Etv1	Gzma
	Tppp3	Nkg7	Ephx1	Nrarp
	Msrb3	Dnajb4	Ptrf	Tspan7
	Gprc5a	Prf1	Ets1	Cd163
	Crim1	Id3	Cd81	Hes1
	Serpinb8	Hey1	Tnfsf13b	Hspa1b
	Crip2	Slc28a2	Pdlim1	Dnajb1
	Hbegf	Nedd4	Il1a	Il2rb
	Cyr61	Igfbp4	Myl3	Cd207
	Fzd4	Dnaja1	Sult1a1	Bcam
	Gpihbp1	Grap	Xlr	

Table S5. Related to Figure 5 **64 differentially expressed genes: St St vs MI cDC1s and cDC2s**

Up-regulated		Down-regulated		
Flot1	Tmem159	Sertad1	Phlda1	Dok2
Ifitm1	Bbc3	Tns1	Lmna	Tinagl1
Casp6	Lyz2	Gbp2	Plxdc2	Sparc
0610040J01Rik	Treml4	Slc5a3	Tnfaip2	Rgs4
Tmem173	Trf	Aldh1a2	Kitl	
Jak3	Ncr1	Cd300lg	Col4a1	
Zdhhc23	Efnb2	Adgre1	Ace	
Itga6	Hmox1	Atp8b1	Zfand2a	
Smad7	Ccl9	Cers4	Sdc1	
Gpr4	Wnt11	Plau	Ltb4r1	
Ctnnd2	Pde2a	Gfra2	Mmp19	
Gpr171	Hsp90aa1	Slc11a1	Mamdc2	
Ggt5	Otof	Steap4	Aplnr	
Syt11	Atf4	Gimap4	Lpl	
Ubr4	Rasl11b	Gypc	Serpinb10	

Table S6. Related to Figure 5 **40 differentially expressed genes: St St vs MI cDC1s and moDCs**

Down-regulated				
Bcl6b	Tnni3	Cd34	Gm13889	Epas1
S100a16	Mb	Cald1	Lims2	Ly6c1
Fam101b	Rasl12	Aqp7	Cav1	She
Fam65b	Adgrg1	Mgll	Ltbp4	Mustn1
Ebi3	Itga7	Alpl	Rhoj	Serpinh1
Hs3st1	Afap1l1	Apold1	Tmem47	Tpm2
Egfl7	Myl9	Tmem204	Nrip2	Gja5
Slc2a4	Ly6a	Nppa	Ablim1	Tagln

Table S7. Related to Figure 5 **105 differentially expressed genes: St St vs MI cDC2s and moDCs**

Up-regulated		Down-regulated		
Fxyd7	St3gal1	Adamts1	Hepacam2	P3h2
Cdh1	Adrb2	Acta2	Dmpk	Rnf144a
Zbtb18	Ctsf	Tmcc1	Slc12a2	Cyp2ab1
Lgi4	Id1	Mxra7	Slc15a2	F13a1
2900026A02Rik	Bank1	Oasl1	Lrrc3	Cd226
Galnt6	Gbp9	Gm6297	Ly6c2	Fcrls
Angptl2	Cxx1c	BC035044	Cdc42ep2	Cd36
Spon1	Tsc22d3	Cracr2b	Klra2	Lyz1
Il18rap	Maf	Cd209d	Ear2	Kcnq1
Arhgap24	St3gal6	Celf4	Cd209b	Cd2
Gcnt1	Icam2	Tmem26	Trpm2	Hspb1
Il7r	Klhl13	Hcar2	Crym	Hpgd
Aatk	Clec4f	Fabp4	Agpat3	Retnla
Scin	Folr2	Cish	Lck	
Tmem158	Gcc1	Gm14085	Sgce	
Plxnc1	Itga9	Ndnf	Adgre4	
Slc7a11	Nos3	Slco2b1	Tlr12	
Nxpe5	Adrb1	Cp	Lilra5	
Stat4	Adgre5	Tppp	Timp3	
Ifit2	Sh3bp5	Adamdec1	Ptgs1	
Map4k3	Alox15	Pf4	Mmp13	
Dock5	1810011O10Rik	Ehd2	Il6	
Anpep	Gbp4	Spic	Itgal	

Table S8. Related to Figure 6 **Differentially expressed genes (high stringency): St St vs MI cDC2s**

Up-regulated		Down-regulated	
Plekha5	Prss30	Tnfaip6	Plcb1
Fads2	Ffar4	Hnmt	Spink2
Tbc1d16	Hpgds	Fgd4	Galnt9
Cst7	Spint2	Tnfaip8l1	9830107B12Rik
Klrb1f	Hivep2	Gfi1b	Tlr7
Siglece	Pvrl4	Fgd6	Nupr1
Myo1b	St8sia6	Steap3	4930455G09Rik
Adam11		Cebpe	Tmem229a

Supplemental Experimental Procedures

Flow cytometric analysis and sorting

Following Abs were used: CD3 (145-2C11), CD19 (1D3), CD45.2 (104), MHC class II (M5/114), CD11c (N418), CD64 (X54-5/7.1), XCR-1 (ZET), CD172α (P84), CD26 (H194-112), Flt3 (A2F10), CD11b (M1/70), CD103 (2E7), CD24 (M1/69), CADM1 (CM004-3), MerTK (polyclonal), FcεR1 (MAR-1), CCR2 (475301), F4/80 (BM8), IRF4 (M-17), IRF8 (C-19), CD4 (RM4-5), V alpha 2 chain (B20.1), V beta 8.1 8.2 chain (MR5-2), CD90.1 (OX-7), T-bet (4B10), RoRγt (Q31-378), Foxp3 (FJK-16s), CD25 (PC61), CD44 (IM7), CD86 (PO3), CD40 (3/23) and CD80 (16-10A1).

RNA sequencing

Trimmomatic was utilized for the preprocessing of the RNA-seq data. The adapters were cut off. Reads were clipped when the quality fell below 20 and were rejected when longer than 35. FastQC was performed and all samples passed quality control. Reads were plotted to the mouse reference genome via Tophat2 and calculated via HTSeqCount. R/Bioconductor was utilized to analyze the samples and data normalization was performed using the DESeq2 procedure. To identify unique cDC2 genes we filtered the normalized log2 expression table using the R package 'sqldf'. Log2 expression of cDC2s from MI heart needed to be at least 1,2 log2 value bigger than cDC2s from steady state heart. The differences between the other steady state and MI samples (cDC1s, moDCs and MFs) needed to be lower than 0,3 log2 value. Gene Set Enrichment Analysis (GSEA) were performed using GSEA GUI v2.2.3 of the Broad Institute (http://software.broadinstitute.org/gsea/downloads.jsp). We used GSEA Pre-Ranked analysis with default parameters and used all genes ordered by LogFC (MI vs StSt, upregulated gene is upregulated in MI) as ranked list.